CarbonTracker-CH_4 Documentation

CT-CH_4 2023 release

Published on September 30, 2023

Youmi Oh[1,2]*, Lori Bruhwiler[1]*, Xin Lan[1,2], Sourish Basu[3], Kenneth Schuldt[1,2], Kirk Thoning[1], Sylvia Englund Michel[4], Reid Clark[4], John B. Miller[1], Arlyn Andrews[1], Owen Sherwood[5], Giuseppe Etiope[6], Monica Crippa[7,22], Licheng Liu[8,9], Qianlai Zhuang[8], James Randerson[10], Guido van der Werf[11], Tuula Aalto[12], Stefano Amendola[13], Sébastien Conil Andra[14], Marcos Andrade[15,57], Nhat Anh Nguyen[16], Shuji Aoki[17], Francesco Apadula[18], Ikhsan Buyung Arifin[19], Sabrina Arnold[20], Mikhail Arshinov[21], Bianca Baier[1], Peter Bergamaschi[7], Tobias Biermann[23], Sebastien C. Biraud[24], Pierre-Eric Blanc[25], Gordon Brailsford[26], Huilin Chen[27], Aurelie Colomb[28], Cedric Couret[29], Paolo Cristofanelli[30], Emilio Cuevas[31], Łukasz Chmura[58], Marc Delmotte[32], Lukas Emmenegger[33], Gulzhan Esenzhanova[34], Ryo Fujita[35], Luciana Gatti[36], Elise-Andree Guerette[49], László Haszpra[37], Michal Heliasz[23], Ove Hermansen[38], Jutta Holst[39], Tatiana Di Iorio[40], Armin Jordan[41], Müller-Williams Jennifer[46], Anna Karion[42], Teruo Kawasaki[43], Victor Kazan[32], Petri Keronen[52], Seung-Yeon Kim[45], Tobias Kneuer[46], Katerina Kominkova[47], Elena Kozlova[48], Paul Krummel[49], Dagmar Kubistin[46], Casper Labuschagne[50], Ray Langenfelds[49], Olivier Laurent[14], Tuomas Laurila[12], Haeyoung Lee[26,45], Irene Lehner[23], Markus Leuenberger[51], Matthias Lindauer[46], Morgan Lopez[32], Reza Mahdi[19], Ivan Mammarella[52], Giovanni Manca[7], Michal V. Marek[47], Martine De Mazière[53], Kathryn McKain[1], Frank Meinhardt[54], Charles E. Miller[55], Meelis Mölder[39], John Moncrieff[56], Heiko Moosen[41], Caisa Moreno[57], Shinji Morimoto[17], Catherine Lund Myhre[38], Alberth Christian Nahas[19], Jaroslaw Necki[58], Sylvia Nichol[26], Simon O'Doherty[59], Nina Paramonova[60], Salvatore Piacentino[40], Jean Marc Pichon[28], Christian Plass-Dülmer[46], Michel Ramonet[32], Ludwig Ries[29], Alcide Giorgio di Sarra[40], Motoki Sasakawa[61], Daniel Say[59], Hinrich Schaefer[26], Bert Scheeren[27], Martina Schmidt[32], Marcus Schumacher[41], Mahesh Kumar Sha[53], Paul Shepson[62], Dan Smale[26], Paul D. Smith[63], Martin Steinbacher[33], Colm Sweeney[1], Shinya Takatsuji[43], Gaston Torres[64], Kjetil Tørseth[38], Pamela Trisolino[30], Jocelyn Turnbull[65], Karin Uhse[29], Taku Umezawa[61], Alex Vermeulen[39], Isaac Vimont[1], Gabriela Vitkova[47], Hsiang Jui Ray Wang[66], Doug Worthy[67], and Irène Xueref-Remy[68]

1 NOAA Global Monitoring Laboratory, Boulder, Colorado, USA
2 CIRES, University of Colorado, Boulder, Colorado, USA
3 Global Modeling and Assimilation Office, NASA Goddard Space Flight Center, Greenbelt, Maryland, USA
4 Institute of Arctic and Alpine Research, University of Colorado, Boulder, Colorado, USA
5 Department of Earth and Environmental Sciences, Dalhousie University, Halifax, Nova Scotia, Canada
6 Istituto Nazionale di Geofisica e Vulcanologia, Rome, Italy
7 European Commission, Joint Research Centre, Ispra, Italy
8 Department of Earth, Atmospheric, and Planetary Sciences, Purdue University, West Lafayette, Indiana, USA
9 The University of Minnesota, Twin City, Minnesota,USA
10 Department of Earth System Science, University of California, Irvine, California, USA
11 Meteorology and Air Quality Group, Wageningen University and Research, Wageningen, the Netherlands
12 Finnish Meteorological Institute, Climate System Research, Helsinki, Finland
13 Italian Air Force Mountain Centre, Sestola, Italy
14 ICOS Atmospheric Thematic Centre, Gif-sur-Yvette, France
15 Department of Atmospheric and Oceanic Science, University of Maryland, College Park, Maryland, USA
16 Viet Nam Meteorological and Hydrological Administration, Hà Nội, Vietnam
17 Tohoku University, Sendai, Japan
18 Ricerca sul Sistema Energetico (RSE) S.p.A., Milano, Italy
19 Badan Meteorologi, Klimatologi, dan Geofisika, Jakarta, Indonesia
20 Deutsches Zentrum für Luft- und Raumfahrt (DLR), Institut für Physik der Atmosphäre, Oberpfaffenhofen, Germany
21 Institute of Atmospheric Optics, Tomsk, Russia
22 Unisystems S.A, Milan, Italy
23 Lund University, Centre for Environmental and Climate Science, Lund, Sweden
24 ARM Carbon Project, Lawrence Berkeley National Laboratory, Berkeley, California, USA
25 University of Reims Champagne-Ardenne, CNRS, Reims, France
26 National Institute of Water and Atmospheric Research, Wellington/Lauder, New Zealand
27 Centre for Isotope Research, University of Groningen, Groningen, Netherlands
28 Clermont-Ferrand Earth Physics Observatory (OPGC), Clermont-Ferrand, France
29 German Environment Agency (UBA), Zugspitze, Germany
30 Institute of Atmospheric Sciences and Climate (CNR-ISAC), Bologna, Italy
31 Agencia Estatal Meteorologia, Santa Cruz de Tenerife, Spain
32 Laboratoire des Sciences du Climat et de l'Environnement, LSCE/IPSL, CEA-CNRS-UVSQ, Université Paris-Saclay, Gif-sur-Yvette, France
33 Empa, Swiss Federal Laboratories for Materials Science and Technology, Laboratory for Air Pollution/Environmental Technology, Dübendorf, Switzerland
34 Agency on Hydrometeorology under Ministry of Emergency Situations of the Kyrgyz Republic, Kyrgyzstan
35 Meteorological Research Institute, Tsukuba, Japan
36 National Institute for Space Research (INPE), Sao Paulo, Brazil
37 Institute for Nuclear Research (ATOMKI), Hungary
38 NILU-Norwegian Institute for Air Research, Kjeller, Norway
39 ICOS Carbon Portal, Lund University, Lund, Sweden
40 Italian National Agency for New Technologies, Energy and Sustainable Economic Development, UTMEA-TER Earth Observations and Analyses Laboratory, Rome, Italy
41 Max Planck Institute for Biogeochemistry, Jena, Germany
42 National Institute of Standards and Technology, Gaithersburg, Maryland, USA
43 Japan Meteorological Agency, Tokyo, Japan
44 University of Helsinki, Helsinki, Finland
45 Korea Meteorological Administration, Seoul, South Korea
46 DWD Meteorological Observatory, Hohenpeißenberg, Germany
47 Global Change Research Institute (CAS), Brno, Czech Republic

48 University of Exeter, Centre for Environmental Data Analysis, Exeter, Devon, United Kingdom
49 Commonwealth Scientific and Industrial Research Organisation (CSIRO), Aspendale, Australia
50 South African Weather Service, Cape Point, South Africa
51 Climate and Environmental Physics, University of Bern, Bern, Switzerland
52 Institute for Atmospheric and Earth System Research/Physics, Faculty of Sciences, University of Helsinki, Finland
53 Royal Belgian Institute for Space Aeronomy (BIRA-IASB), Brussels, Belgium
54 Umweltbundesamt, Messstelle Schauinsland, Kirchzarten, Germany
55 Jet Propulsion Laboratory, California Institute of Technology, Pasadena, California, USA
56 Institute of Ecology and Resource Management, University of Edinburgh, Edinburgh, UK
57 Laboratory for Atmospheric Physics, Institute for Physics Research, Universidad Mayor de San Andrés, La Paz, Bolivia
58 AGH - University of Kraków, Kraków, Poland
59 University of Bristol, Bristol, United Kingdom
60 Voeikov Main Geophysical Observatory,Saint Petersburg, Russia
61 National Institute for Environmental Studies, Tsukuba, Japan
62 Purdue University, West Lafayette, Indiana, USA
63 Swedish University of Agricultural Sciences, Svartberget Field Research Station, Vindeln, Sweden
64 Chilean Meteorological Service (Dirección Meteorológica de Chile, DMC), Chile
65 GNS Science,National Isotope Centre, Lower Hutt, New Zealand
66 Georgia Institute of Technology, Atlanta, GA, USA
67 Environment and Climate Change Canada, Ontario, Canada
68 Aix Marseille Univ, Avignon Université, CNRS, IRD, IMBE (Institut Méditerranéen de Biodiversité et d'Ecologie marine et continentale), Aix/Marseille, France

Contents

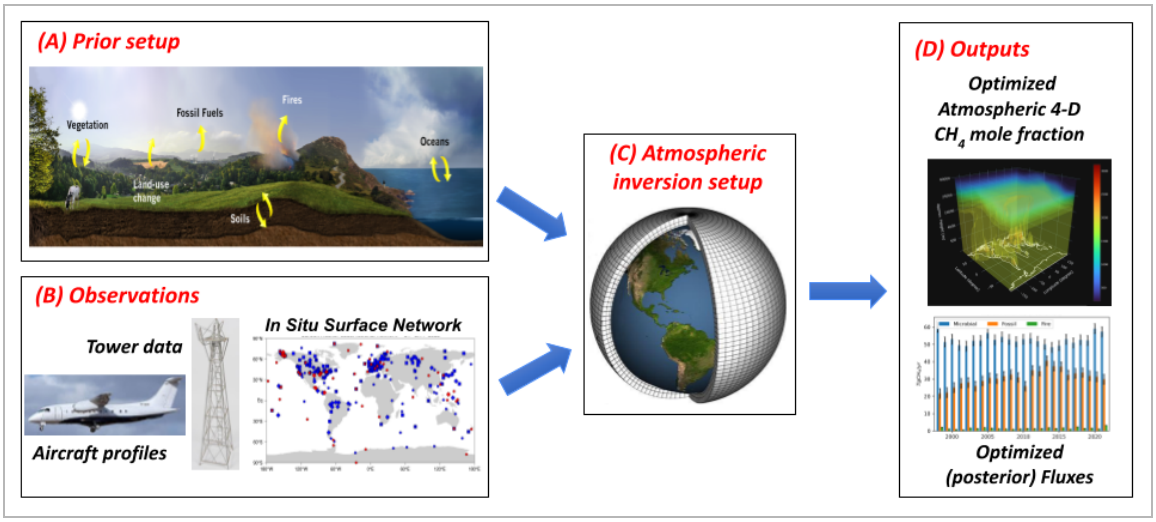
(A) Prior setup
Vegetation
Fossil Fuels
Fires
Oceans
Land-use change
Soils
(B) Observations
Tower data
In Situ Surface Network
Aircraft profiles
(C) Atmospheric inversion setup
(D) Outputs
Optimized Atmospheric 4-D CH_4 mole fraction
Optimized (posterior) Fluxes

The goal of the CarbonTracker-CH_4 is to produce quantitative estimates of methane (CH_4) emissions at the Earth's surface that are consistent with observed patterns of CH_4 and its stable carbon isotope ratios ($\delta^{13}C$-CH_4) in the atmosphere. CarbonTracker-CH_4 is an dual-tracer inverse model of atmospheric CH_4 and $\delta^{13}C$-CH_4, which means that it produces model predictions of atmospheric CH_4 and $\delta^{13}C$-CH_4, to be compared with the observed atmospheric CH_4 and $\delta^{13}C$-CH_4 (**Section B**). The difference between them is attributed to differences in the emissions used to make the prediction (prior) and emissions affecting the true atmospheric CH_4. Using numerical techniques (**Section C**), these differences are used to solve for a set of emissions that most closely matches the observed CH_4 and $\delta^{13}C$-CH_4 in the atmosphere (posterior). CarbonTracker-CH_4 has a representation of atmospheric transport based on weather forecasts, and modules representing emissions from microbial, fossil, and pyrogenic sources, and oxidation by atmospheric chemical reactions and soil microbes (**Section A**). The outputs include global 3-D mole fraction of atmospheric CH_4, monthly estimation of microbial, fossil, and pyrogenic sources, and pre-processed observations of atmospheric CH_4 and $\delta^{13}C$-CH_4 used for Carbontracker-CH_4 (**Section D**). CarbonTracker-CH_4 is updated on an approximately annual basis, and the current release, CT-CH_4 2023, provides results from 1997 through the end of 2021.

A. Prior setup

1. Prior emissions

Prior estimates of emissions from microbial, fossil, and pyrogenic sources are based on bottom-up inventories and process-based models (Figure 1 and Table 2). **Our current inversion approach is to estimate fluxes from total microbial, fossil, and pyrogenic sources, rather than estimating each source sector separately** (Basu et al. 2022)**. Our use of atmospheric isotope data allows observational constraints on the partitioning between fossil and microbial emissions, but little information on how emissions are distributed among the source sectors (e.g. anthropogenic and natural microbial sources).** Based on the posterior mean estimates of global methane (CH_4) emissions, about 35% of CH_4 emissions is from anthropogenic microbial sources, 30% is from natural microbial sources, 30% is from fossil sources, and 5% is from pyrogenic sources (Figure 1). Detailed information on each source sector can be found in the following sections.

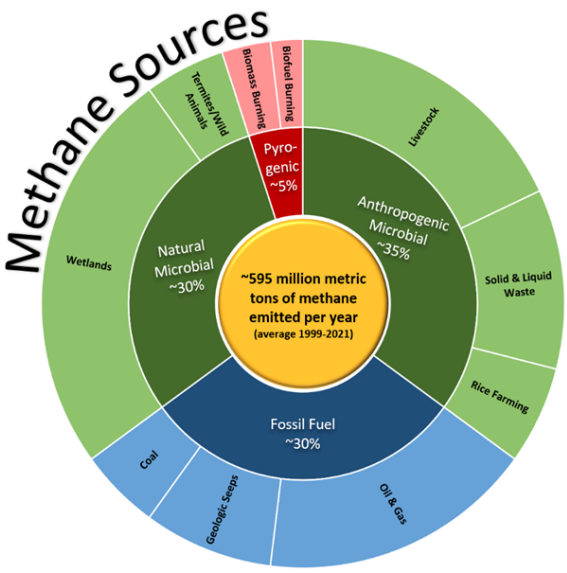

Figure 1. Estimated mean global CH_4 emissions from microbial, fossil, and pyrogenic source sectors. Credit: Amy Leibrand.

1.1. Microbial

1.1.1. Anthropogenic microbial (e.g. ruminants, waste, and rice)

Agriculture is the most significant source of CH_4 emitted by human activity (200-240 $TgCH_4/yr$) (Saunois et al. 2020). Ruminants, such as cattle, goats, sheep, and buffalo can convert hard-to-digest forage to energy through a process called enteric fermentation, in which microbes produce easily digested material inside the animal's gut. Most of the CH_4 produced in this way exits the animal via belching, however, a small portion emerges from flatulence. CH_4 emissions from animals can be reduced by the use of more easily digested feed, and research to develop dietary supplements targeted at reducing these emissions is ongoing (Abbott et al. 2020). Emissions from enteric fermentation are expected to increase as the global population and affluence grows.

Animal waste, wastewater, and landfills produce CH_4 when conditions favor anaerobic decomposition. This is the process by which organic material decomposes in low oxygen conditions by chains of microbial processes that produce mostly CH_4 and carbon dioxide (CO_2). CH_4 produced in landfills or waste treatment facilities can be captured and used as fuel rather than being vented into the atmosphere (Themelis and Bourtsalas 2021).

Rice agriculture is also a significant source of CH_4 in the atmosphere. This is because warm, waterlogged rice paddies are ideal for the development of anaerobic conditions and methanogenesis. Bottom-up estimates of emissions from rice agriculture are about

25-40 $TgCH_4$/yr (Saunois et al. 2020), and emissions can be significantly reduced by drainage of paddies between harvests, application of fertilizer, and development of varieties of rice that tolerate drier conditions.

This release of CarbonTracker-CH_4 uses the 1x1 degree gridded emissions from EDGAR 4.3.2 as prior emission estimates for emissions from rice agriculture, enteric fermentation, animal waste management, wastewater, and landfills (Janssens-Maenhout et al. 2019). After 2007, we applied globally-uniform scale factors on microbial sources that satisfy global mass balance (**Section A4**).

1.1.2. Natural microbial (wetlands, wild animals, termites, and other aquatic sources)

The largest source of CH_4 from natural sources is wetlands. Wetlands are defined as regions that are permanently or seasonally waterlogged, and they can be broadly categorized into marshes, swamps, bogs and fens. Wetlands include both high-latitude peat bogs and typically low-latitude tropical swamps. Saturated soils in warm tropical environments tend to produce the most CH_4, however, warming Arctic temperatures raise concern for increasing output from high-latitude wetlands and future decomposition of carbon that is currently stored in the frozen soils of the Arctic (Schuur et al. 2022; Zhang et al. 2023).

CH_4 is easily oxidized in overlying aerobic water columns or wetlands. Because of this, for a wetland to be most productive, the water table must be at or near the surface or the depth of overlying water must be shallow, or plants with aerenchyma acts as a rapid path to bypass the oxic surface layers (Le Mer and Roger 2001; McNicol et al. 2023). Over time, wetland plants have adapted to low oxygen environments with hollow stems to allow the delivery of oxygen and other gases to their root systems. These hollow stems also allow transport of CH_4 directly to the atmosphere, which along with bubbles, accounts for most of the CH_4 transport into the atmosphere. Diffusion also occurs but is thought to be significantly smaller. Estimates of global emissions from wetlands are about 100-200 $TgCH_4$/yr with most coming from tropics (Saunois et al. 2020), which we hope to narrow with CarbonTracker-CH_4. Most of this occurring in tropical regions. Because emissions are sensitive to temperature and precipitation, they exhibit significant seasonal cycles (especially at high latitudes) and inter-annual variability (Zhang et al. 2017).

Other natural sources of CH_4 include enteric fermentation in insects (mainly termites) and wild animals. Both of these sources are thought to be much smaller than that from wetlands (10-25 $TgCH_4$/yr) (Bergamaschi et al. 2007; Lan et al. 2021).

Recent studies found that CH_4 emissions from aquatic ecosystem sources are largely underestimated (Rosentreter et al. 2021). Since the estimation of aquatic sources is highly uncertain (25 to more than 200 $TgCH_4/yr$) (Saunois et al. 2020; Zhuang et al. 2023), the aquatic sources were not considered for this release of CarbonTracker-CH_4.

CH_4 emissions from wetlands are difficult to quantify for two reasons; their global spatial distribution is difficult to accurately pinpoint and there is large variability in conditions that lead to CH_4 production. This release of CarbonTracker-CH_4 uses the 1x1 degree gridded wetland emissions of CH_4 from a process-based model, a Terrestrial Ecosystem Model (TEM) (Zhuang et al. 2004; Liu et al. 2020), that use global static wetland distribution from (Matthews and Fung 1987).

1.2. Fossil

Humans first began influencing the carbon cycle by adapting their environment to fit their needs. Early humans used fire to control animals and later cleared forests for agriculture. Over the last two centuries, following the industrial and technical revolutions as well as a significant increase in global population, fossil fuel combustion is now the largest anthropogenic source of CO_2 (Crippa et al. 2020). Coal, oil, and natural gas are the most common energy sources.

CH_4 is the principal component of natural gas. It leaks to the atmosphere during natural gas production and transport, and these leaks contribute a considerable amount to atmospheric CH_4 levels. Natural gas can also be a side product of oil production that is flared, or vented to the atmosphere. Together, anthropogenic emissions from oil and gas production are thought to contribute about 70-100 $TgCH_4/yr$ (~10% of the global annual CH_4 sources) based on bottom-up inventories (Saunois et al. 2020). CH_4 is also associated with coal deposits and can be released when pulverizing coal, an important step in preparing coal for power production. However, the largest contribution from coal production is venting directly to the atmosphere from coal mines. Emissions from coal may contribute an additional 30-60 $TgCH_4/yr$.

As of 2022, coal supplied only about 20% to national electricity generation, and its share has been dropping as natural gas and renewables have become less expensive (https://www.eia.gov/tools/faqs). Coal has high environmental costs; leveling of mountaintops, pollution of waterways, emissions of sulfur and nitrogen oxides, as well as mercury are all associated with coal production and combustion. In addition, the amount of CO_2 emitted per unit of energy produced is about twice that of natural gas, making coal an environmentally costly choice for energy production (Ren and Patel 2009). China is the world's largest consumer of coal, followed by India and the U.S. In

China, coal supplied about 55% of China's total energy consumption in 2021, and China's fossil consumption has increased by more than a factor of three over the last two decades (https://www.eia.gov/international/analysis/country/CHN).

Combustion of natural gas currently generates 60% of electricity in the U.S in 2022 (https://www.eia.gov/tools/faqs/faq.php?id=427&t=3). Its popularity as a fuel has grown due to its efficiency and lower air quality and climate impacts. Advances in recovery of natural gas, principally hydraulic fracturing, have led to increases in reserve estimates. It is now thought that the U.S. has a large enough natural gas supply to last nearly a century based on current consumption. U.S. shale gas production accounted for 80% of the global shale gas production in 2022 (https://www.eia.gov/tools/faqs/faq.php?id=907&t=8).

Lastly, natural fossil CH_4 can be emitted from geologic seeps in shallow coastal waters (Etiope et al. 2019). In order for this to happen, the overlying water column must be shallow since CH_4 is efficiently removed by anaerobic microbial processes. This means that the water column must be shallow enough for bubbles to deliver CH_4 directly to the air at the surface, called ebullition. Fossil CH_4 can also be emitted from terrestrial seeps and other features such as mud volcanoes and hot springs. Estimates of the contribution of geologic emissions vary from negligible to 40-60 Tg CH_4/yr or more, making this process highly uncertain (Judd 2004; Saunois et al. 2020).

This release of CarbonTracker-CH_4 uses the 1x1 degree gridded emissions from the EDGAR 4.3.2 as prior emission estimates for anthropogenic fossil fuel emissions (Janssens-Maenhout et al. 2019). Since this dataset is available until 2012, we kept prior fossil emission estimates constant at 2012 levels. We use natural fossil emissions reported by (Etiope et al. 2019).

1.3. Pyrogenic (biomass and biofuel burning)

Fire is an important part of the carbon cycle. Even before human civilization began to use fire to clear land for agricultural purposes, most ecosystems were subject to natural wildfires. These fires rejuvenated old forests in various ways including reintroducing important minerals to the soils. As fires consume a landscape, in either controlled or natural burning, CO_2, CO, and CH_4 (among many other gasses and aerosols) are released in significant quantities. Each year, vegetation fires emit around 2 PgC as CO_2 into the atmosphere, mostly in the tropics (Van Der Werf et al. 2017). Fires are a relatively small part of the atmospheric CH_4 budget: ~30 TgCH_4/yr, however, they are an important contribution to the inter-annual variability of CH_4 (Randerson et al. 2018). A

large fraction of present-day fires are started by humans, with most started intentionally to clear land for agriculture, or to re-fertilize soils before a new growing season.

For biomass and biofuel burning emissions of this CarbonTracker-CH_4 release, we use the Global Fire Emission Database (GFED) 4.1s for 1997–2021 (Van Der Werf et al. 2017).

2. Isotopic signatures of emission sources

The stable carbon isotopic ratios (in delta notation, $\delta^{13}C\text{-}CH_4$) describes the ratio of the heavy isotope to the light isotope in the sample ($R_{sam}=(^{13}C/^{12}C)_{sam}$) relative to a known standard ratio, R_{std}, which is Vienna Pee Dee Belemnite (VPDB) for carbon (Equation below). The deviation of this ratio-of-ratios from one is multiplied by 1000 to express isotope variations in parts per thousand (‰, permil).

$$\delta^{13}C = (R_{sam}/R_{std})-1$$

Measurements of atmospheric CH_4 abundance and $\delta^{13}C\text{-}CH_4$, in combination with isotopic signatures of sources and sinks, allow partitioning of CH_4 budgets into different source categories. This is because isotopic signatures of source categories differ significantly, where the $\delta^{13}C\text{-}CH_4$ of microbial sources (−61.7±6.2‰) is isotopically more depleted (i.e. more of the lighter carbon isotope) than fossil (−44.8±10.7‰) and biomass burning (−26.2±4.8‰) sources (Sherwood et al. 2021). When the isotopic signature is weighted by spatiotemporal-varying flux in each emi sector, the mean isotopic signature between microbial, fossil, and pyrogenic sources becomes more separable (Figure 2). More information on our source isotopic signature can be found in (Lan et al. 2021).

Instead of optimizing the source signatures, we fix the signatures based on our best understanding from bottom-up inventories and modeling to reduce the degrees of freedom in our inversion system. In principle, it is possible to estimate both CH_4 fluxes and $\delta^{13}C\text{-}CH_4$ source signatures in a dual tracer inversion. However, this makes the problem non-linear and the inversion convergence slow. It is also difficult to construct a prior covariance for $\delta^{13}C\text{-}CH_4$ source signatures since much of the uncertainty stems from extrapolating a limited number of $\delta^{13}C\text{-}CH_4$ signature measurements to the entire domain of CH_4 sources, resulting in errors that are systematic and non-Gaussian. Therefore, we explore the impact of $\delta^{13}C\text{-}CH_4$ signature uncertainty on our results by running inversions with alternate specifications of $\delta^{13}C\text{-}CH_4$signature maps. Please see details in Basu et al. 2022.

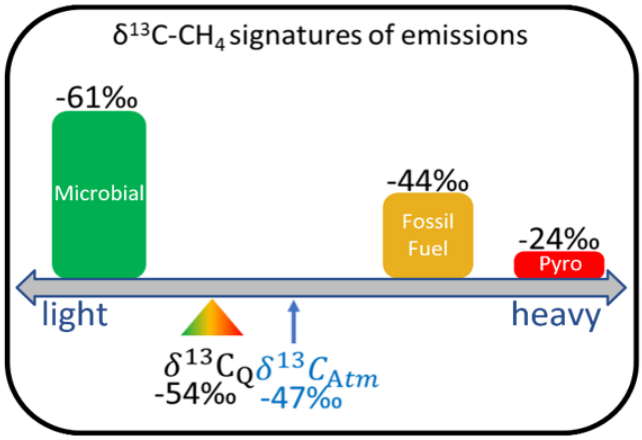

Figure 2. Global mean flux-weighted CH_4 isotopic signature ($\delta^{13}C\text{-}CH_4$) of microbial, fossil, and pyrogenic sources. Approximate values of global mean source signatures are shown. Credit. Xin Lan.

2.1. Microbial

For wetland emissions, the spatial map of $\delta^{13}C\text{-}CH_4$ from (Ganesan et al. 2018) is used, that is based on global C3/C4 vegetation map and soil pH. We use globally averaged $\delta^{13}C\text{-}CH_4$ source signatures for waste/landfills, termites, and rice given insufficient measurement sample size to develop spatial source signature distributions (Sherwood et al. 2017; Sherwood et al. 2021). Ruminant and wild animal source signatures depend strongly on the locally available mix of C3- and C4-based biomass material (Chang et al. 2019). We used the averages of two different global maps of biomass C3/C4 ratios (Randerson et al. 2012; Still et al. 2003) in combination with measurements of C3- and C4-based $\delta^{13}C\text{-}CH_4$ source signatures to create global source signature maps at 1°×1° resolution.

2.2. Fossil

The fossil source $\delta^{13}C\text{-}CH_4$ signatures are also from the datasets by (Sherwood et al., 2021). In these datasets, fossil signatures were categorized by (1) coal gas, (2) conventional gas, and (3) shale gas (Lan et al. 2021). The global gridded map of fossil isotopic signatures is created based on the spatial distribution of available $\delta^{13}C\text{-}CH_4$ signatures. For the U.S. region, we calculate the oil and gas $\delta^{13}C\text{-}CH_4$ mean signature year by year as the average of shale gas and conventional gas signatures for major basins weighted by their respective basin-level gas production volumes at 1°×1°

resolution (Lan et al. 2021). For countries without available fossil $\delta^{13}C\text{-}CH_4$ signature data, global average $\delta^{13}C\text{-}CH_4$ values (weighted by country-level production) are used. The other energy/industry category includes small fossil sources, such as the power industry, combustion for manufacturing, aviation, ground transportation and shipping, and iron and steel production, and we use the global weighted average fossil fuel isotopic signature for this category. A spatially resolved global map of $\delta^{13}C\text{-}CH_4$ signatures from geological seepage was developed by (Etiope et al. 2019) and used in this project.

2.3. Pyrogenic

Biomass burning and biofuel burning $\delta^{13}C\text{-}CH_4$ is dependent strongly on the locally available mix of C3- and C4-based biomass material (for combustion or as a food source). Here, we used the averages of two different global maps of biomass C3/C4 ratios (Randerson et al. 2012; Still et al. 2003) in combination with measurements of C3- and C4-based $\delta^{13}C\text{-}CH_4$ source signatures to create global source signature maps at 1° × 1° resolution.

3. Chemical and Soil Sinks of Methane

3.1. Distribution and magnitude

Atmospheric CH_4 has three loss mechanisms: atmospheric oxidation by OH and Cl throughout the atmosphere, destruction by $O(^1D)$ in the stratosphere, and surface uptake in aerobic soils (Figure 3) (Basu et al. 2022; Lan et al. 2021). Atmospheric oxidation of CH_4 in the tropospheric OH and Cl is the largest portion of CH_4 sources (87%), and the atmospheric oxidation in the stratosphere accounts for about 7% of the total CH_4 sinks. A small fraction of CH_4 is consumed by aerobic bacteria in upland soils (6%). **Note: we are not adjusting the chemical sink in this version of Carbontracker-CH_4.**

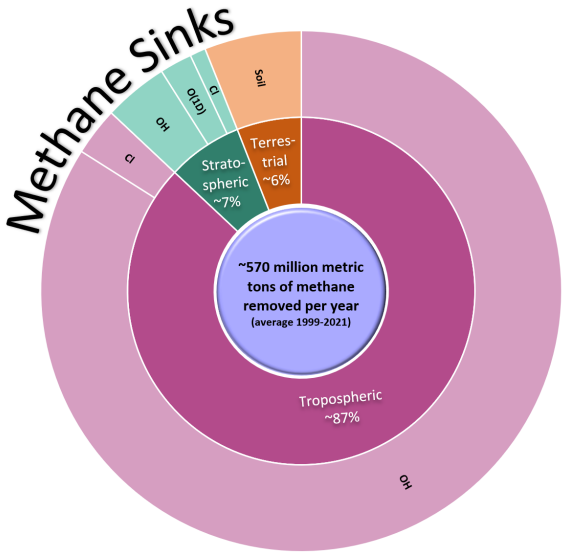

Figure 3. Bar chart of global mean CH_4 sinks from atmospheric chemical reactions and soil sinks. Credit: Amy Leibrand.

3.1.1. Atmospheric chemical reactions

CH_4 is removed from the atmosphere primarily by its reaction with the hydroxyl radical (OH), but also by its reaction with atomic chlorine (Cl) and excited-state oxygen (O^1D) in the stratosphere. Methane is also removed in the troposphere by Cl, but this is a small sink comprising ~3% of total global loss. The distribution of Cl in the troposphere is highly uncertain, but because its reaction with CH_4 is strongly fractionating it can have a large effect on the isotopic composition of atmospheric CH_4 (Strode et al. 2020; Gromov et al. 2018). The chemical loss of CH_4 over a year is roughly equal to the total input from its sources (~570 $TgCH_4$/yr), causing the average lifetime of CH_4 in the troposphere to be much shorter (about 9 years) than CO_2 (> 100 years). However, small differences in the total emissions and losses of CH_4, lead to changes in observed CH_4 levels (Figures 1 and 3).

It is difficult to characterize the global distribution of OH because it is extremely reactive as well as it has a short lifespan within the atmosphere. Instead, observations of atmospheric species that have relatively well-known anthropogenic sources and are destroyed only by reaction with OH, such as methyl chloroform (CH_3CCl_3), are used to estimate the abundance of atmospheric OH. Utilizing an empirical approach, (Montzka et al. 2011) noted that the inter-annual variability in atmospheric OH is likely to be within about ~2%. Errors in OH distributions arise from uncertainty in the sources of CH_3CCl_3 used to estimate OH, as well as uncertainties in transport models (Krol et al. 1998) estimate that the uncertainty of OH distribution is 10%.

About 7% of the total chemical loss of CH_4 is due to transport and breakdown in the stratosphere. A small amount of this CH_4-depleted air is returned to the troposphere and has the potential to influence the interpretation of high-altitude (aircraft) measurements of CH_4 (Zhou et al. 2023). In addition, errors in simulating stratosphere-troposphere transport have the potential to produce biases for long-term model simulations.

Errors in the chemical loss of CH_4, and the inability to adequately resolve inter-annual variability of OH, make the estimation of CH_4 fluxes challenging. A 2% variation in the global CH_4 sink is equivalent to ~10 $TgCH_4$/yr, roughly the size of estimated inter-annual variability in CH_4 sources. Currently, the best approach is to use OH fields that are as consistent as possible with existing records of species whose chemistry is significantly linked with OH. Examples include carbon monoxide (CO) and methyl chloroform (CH_3CCl_3) (Patra et al. 2014).

This release of CarbonTracker-CH_4 prescribes and does not optimize methane sinks. Monthly climatological CH_4 loss rates in the stratosphere due to OH, Cl, and $O(^1D)$ were constructed from a run of the ECHAM5/MESSy1 chemistry transport model (Jöckel et al. 2006). Loss due to tropospheric Cl is simulated using a recent model-derived estimate of tropospheric Cl (Hossaini et al. 2016). For tropospheric OH, we use the monthly OH climatology of (Spivakovsky et al. 2000) after scaling by 0.9 to match the declining atmospheric abundance of methyl chloroform in the early 2000s (Montzka et al. 2011; Basu et al. 2022).

3.1.2. Soil sink of atmospheric CH_4

A natural sink of atmospheric CH_4 is oxidation by microbes in dry soils (~40 $TgCH_4$/yr), but the total size of global soil sinks is uncertain due to undetermined key environmental parameters (Oh et al. 2020; Lee et al. 2023). Wetlands that undergo dry and wet seasons can switch between being sources and sinks of CH_4 as well. This release of CarbonTracker-CH_4 uses the 1x1 degree gridded soil consumption of CH_4 from a process-based model, a Terrestrial Ecosystem Model (TEM) (Zhuang et al. 2013; Liu et al. 2020).

3.2. Fractionation

Each CH_4 sink process shows its different preference for reacting with the light ^{12}C over the heavier ^{13}C (Figure 4). The fractionation between ^{12}C and ^{13}C for each of the sink reactions is modeled as the equation below (Saueressig et al. 2001), where *T* is the air temperature in Kelvin. Coefficients *C* and *D* that we used are tabulated in Table 1.

$$k_{12}/k_{13}=1/\alpha=Ce^{D/T}$$

Compared to (Basu et al. 2022), we changed the OH fractionation factor from 1.0039 (Saueressig et al. 2001) to 1.0054 (Cantrell et al. 1990), because the simulation with the latter fractionation improves representation of the seasonality and latitudinal gradients of observed CH_4 isotopes.

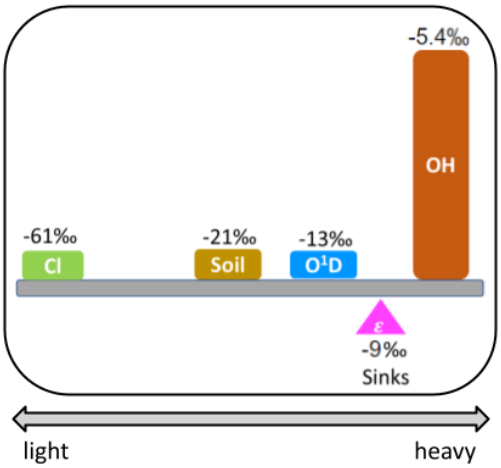

Figure 4. The global mean process-weighted isotopic signature of atmospheric chemical sinks and soil sinks. Credit. Xin Lan.

Table 1. Fractionation parameters for CH_4 sink processes

Loss reaction	**C**	**D(K)**	**Reference**
Loss of OH	1.0054	0.00	(Cantrell et al. 1990)
Loss of Cl	1.0430	6.46	(Saueressig et al. 1995)
Loss of O^1D	1.0130	0.00	(Saueressig et al. 2001)
Soil sink	1.0215	0.00	(King et al. 1989)

4. Global mass balance

Modeling $\delta^{13}C\text{-}CH_4$ in the atmosphere requires special care to spin up the model to a quasi-steady state to avoid initial condition artifacts during the analysis period (Tans, 1997). The time required for atmospheric $\delta^{13}C\text{-}CH_4$ to reach a steady state can be

significantly longer than even the CH_4 lifetime of ~9 years, depending on the size of the atmospheric CH_4 burden and how far off the initial $\delta^{13}C\text{-}CH_4$ is. Thus, we spun up our model for 14 years from 1984 to 1997, and selected 1998–2021 as the analysis period. To further avoid the initial condition artifacts, we adjust our prior to satisfy global mass balance requirements for CH_4 and $\delta^{13}C\text{-}CH_4$ (Lan et al. 2021).

The sum of the bottom-up CH_4 emission estimates described above is not consistent with top-down estimates of global total emissions based on observed atmospheric CH_4 growth and estimated loss, which requires a 67 Tg yr^{-1} increase in the annual global emission in 2021 compared to the 1999–2006 when atmospheric growth was small. In addition, the $\delta^{13}C\text{-}CH_4$ mass balance requires 145 Tg yr^{-1} emissions from fossil sources (including natural geological seeps) to be consistent with observed averaged $\delta^{13}C\text{-}CH_4$ in the atmosphere. Therefore, we (i) scale the oil and gas emissions from EDGAR 4.3.2 to reach a total of 145 Tg yr^{-1} from all fossil sources, and (ii) impose a linear trend on microbial emissions to achieve an increase of 67 Tg yr^{-1} in total 2021 emissions compared to 1999–2006. This ensures that our global CH_4 and $\delta^{13}C\text{-}CH_4$ budgets approximate the long-term trends in atmospheric CH_4 and $\delta^{13}C\text{-}CH_4$ during our simulation period.

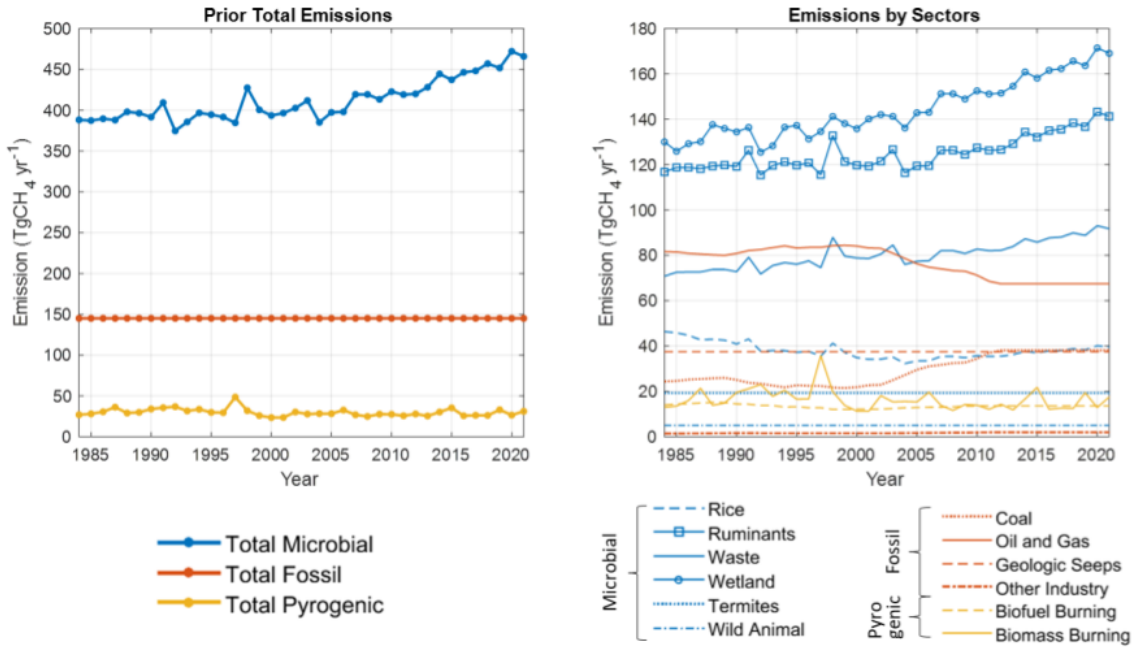

Figure 5. Long-term annual emissions of total microbial, fossil, and pyrogenic sources (left) and each source sector (right) after the global mass balance of atmospheric CH_4 and $\delta^{13}C\text{-}CH_4$.

5. Summary table of data sources for prior sources and sinks

Table 2 summarizes data sources for different CH_4 sources and their source signatures, and table 3 summarizes data sources for different CH_4 sinks and their fractionation factors, that we used for this release of Carbontracker-CH_4.

Table 2. Data sources for total source emissions and δ^{13}C-CH_4 source signatures for this version of CarbonTracker-CH_4.

Source	**Source sector**	**Total emissions**	***δ^{13}C-CH_4 source signatures***
Fossil Emission	Coal, oil and natural gas, and other energy/industry	EDGAR 4.3.2 (Janssens-Maenhout et al. 2019)	(Sherwood et al. 2021)
	Geological seeps	(Etiope et al. 2019)	(Etiope et al. 2019)
Biomass and biofuel burning	Biomass burning fluxes	GFED 4.1s (Randerson et al. 2018; Van Der Werf et al. 2017)	(Randerson et al. 2012; Still et al. 2003)
	Biofuel fluxes	EDGAR 4.3.2 (Janssens-Maenhout et al. 2019)	(Randerson et al. 2012; Still et al. 2003)
Microbial Emission	Ruminants fluxes	EDGAR 4.3.2 (Janssens-Maenhout et al. 2019)	(Randerson et al. 2012; Still et al. 2003)
	Waste and landfills fluxes		(Sherwood et al. 2021)
	Rice fluxes		
	Wild animals and termites fluxes	(Bergamaschi et al. 2007)	

	Wetland and soil sink	Based on (Liu et al. 2020) and static inundation data from (Matthews and Fung 1987).	(Ganesan et al. 2018)

Table 3. Data sources for sink strength/distribution and fractionation for this version of CarbonTracker-CH_4.

Sink	Location	Distribution	Fractionation
Loss of OH	Troposphere	(Spivakovsky et al. 2000); (Montzka et al. 2011)	(Cantrell et al. 1990)
	Stratosphere	(Jöckel et al. 2006)	
Loss of Cl	Troposphere	(Hossaini et al. 2016)	(Saueressig et al. 1995)
	Stratosphere	(Jöckel et al. 2006)	
Loss of O1D	stratosphere	(Jöckel et al. 2006)	(Saueressig et al. 2001)
Soil sink	Terrestrial	(Zhuang et al. 2013; Liu et al. 2020)	(King et al. 1989)

B. Observations

1. Atmospheric CH_4 measurement dataset

To maximize the spatiotemporal coverage of atmospheric data, we utilized database that harmonized measurements from NOAA/INSTAAR with those from 30 other laboratories around the world (Lan et al. 2021; Basu et al. 2022). All CH_4 data have been quality-checked and converted to the World Meteorological Organization (WMO) X2004A scale (Dlugokencky et al. 2005). For data not on the WMO X2004A scale, we applied lab-specific scale multipliers estimated based on comparisons of co-located atmospheric measurements or common air sample experiments. The level of uncertainty in the assimilated CH_4 measurements depends on factors such as the consistency of measurements, their ability to be replicated, and the accuracy of calibration scale implementation. The final measurement uncertainties are typically less than 9 ppb for all CH_4 measurements (Lan et al. 2021).

2. Atmospheric *$\delta^{13}C$-CH_4 measurement dataset*

We used *$\delta^{13}C$-CH_4* data from the Institute for Arctic and Alpine Research (INSTAAR) as well as other isotope laboratories making precise measurements of atmospheric CH_4 with isotope ratio mass spectrometers. The INSTAAR *$\delta^{13}C$-CH_4* data were measured in a subset of air samples collected from NOAA's Global Greenhouse Gas Reference Network (GGGRN). Because different labs have independent ties to primary reference materials which may not agree, we calculated offsets to bring the *$\delta^{13}C$-CH_4* data onto the INSTAAR realization of the Vienna Pee Dee Belemnite (VPDB) scale (Miller et al. 2002). These offsets were based on measurements of cylinders, flasks filled from cylinders, or co-located sample data, and are all described in (Umezawa et al. 2012). When there was not a direct comparison, we used comparisons between each of these labs and the Institute for Marine and Atmospheric research Utrecht (IMAU). Each comparison had an uncertainty associated with it, and these were combined in quadrature to account for uncertainty in the offset correction. The total measurement uncertainty in assimilated *$\delta^{13}C$-CH_4* datasets was typically less than 0.15 ‰.

3. *Selection of assimilated dataset*

With the following exceptions, we assimilate all the observations from this database including marine boundary layer sites, surface and tower sites over continents (Andrews et al. 2014), and vertical profiles from routine aircraft measurements (Sweeney et al.

2015) (Basu et al. 2022). Intermittent aircraft profiles such as from the HIPPO (Wofsy 2011) and ATom (Thompson et al. 2022) campaigns are not assimilated. CH_4 data from flasks taken aboard routine flights between Japan and Australia as part of the CONTRAIL program have been assimilated (Saitoh et al. 2015). A subset of the CONTRAIL flasks was also analyzed for $\delta^{13}C\text{-}CH_4$ (Umezawa et al. 2012), which were not assimilated. For continental tower sites with multiple intake heights, only data from the highest intake are considered in inversions to minimize influence of local sources. For sites with continuous CH_4 analyzers, the CH_4 data are averaged hourly, and only hourly averages between 11:00 and 16:00 local solar time are assimilated; these are the times when planetary boundary layer heights are likely to be best represented by transport models. For continuous CH_4 analyzers on mountain tops, we only assimilate hourly averages between 00:00 and 05:00 local solar time to avoid possible up-slope contamination. Site-specific statistical filtering based on a nonparametric curve fitting routine is further applied, with the exception of vertical profiles, to remove large outliers with potential local or other contamination. The summary of all assimilated and unassimilated sites is in Tables 4-5.

4. *Model-data mismatch setup*

We set model-data mismatch for CH_4 and $\delta^{13}C\text{-}CH_4$ differently. For CH_4, we followed the method from (Bruhwiler et al. 2014). Specifically, the model–data mismatch values for CH_4 were based on the evaluation of forward simulation with prior fluxes by selecting the one standard deviation of prior bias (prior - observed) for each surface site. For aircraft profiles, model-data mismatch was determined using the one standard deviation of the prior bias at every 1 km vertical interval. We forced the assimilation to closely match remote marine background sites while some sites were given a very large model–data mismatch because they are likely influenced by strong local sources. A complete list of sites and their model–data mismatches for CH_4 sites is shown in Table 4.

For $\delta^{13}C\text{-}CH_4$, we followed the method from (Bergamaschi et al. 2005; Basu et al. 2022). In specific, the model-data mismatch is calculated as the quadrature sum of measurement errors and model errors. We calculated model error by calculating the spatial gradient of modeled $\delta^{13}C\text{-}CH_4$ at the monitoring sites, using horizontally and vertically adjacent model grid cells. A complete list of sites and their model–data mismatches for $\delta^{13}C\text{-}CH_4$ sites is shown in Table 5.

Table 4. Summary of statistics of observational Sites for CH_4 used in CarbonTracker-CH_4.

Assimilated										
	Site Code	Laboratory	Latitude	Longitude	Elevation (MASL)	No. of Observation	Model-data mismatch	Mean bias	Standard deviation of bias	Chi-squared
1	ABP ch4 surface event INPE	INPE	-12.77	-38.17	15	186	7.82	-2.96	7.94	1.17
2	ABP ch4 surface event NOAA	NOAA	-12.77	-38.17	6	222	5.42	-0.26	5.71	1.11
3	ABT ch4 surface hourly EC	EC	49.01	-122.34	93	51389	40.89	-40.27	40.6	1.96
4	ALF ch4 aircraft event INPE	INPE	-8.86	-56.75	2229.37	1931	15.11	1.05	15.79	1.07
5	ALK ch4 aircraft event TU	TU	65.89	-152.1	2067.39	64	13.86	-1.05	9.85	0.47
6	ALT ch4 surface event MPI-BGC	MPI-BGC	82.45	-62.51	185	432	12.85	4.22	8.1	0.5
7	ALT ch4 surface event NOAA	NOAA	82.45	-62.51	190	3562	13.45	2.61	9.07	0.49
8	ALT ch4 surface hourly EC	EC	82.45	-62.51	195	150696	12.66	3.57	8.93	0.58
9	AMS ch4 surface event LSCE	LSCE	-37.8	77.54	72.61	882	5.27	-0.25	3.81	0.5
10	AMS ch4 surface hourly LSCE	LSCE	-37.8	77.54	75	12761	5	1.66	2.19	0.3
11	AMT ch4 surface event NOAA	NOAA	45.03	-68.68	160.11	2259	23.34	-3.55	14.7	0.43
12	AMY ch4 surface event NOAA	NOAA	36.54	126.33	87	804	47.13	3.2	33.23	0.5
13	AMY ch4 surface hourly KMA	KMA	36.54	126.33	47	148695	58.15	-6.89	52.49	0.83
14	AOA ch4 aircraft event JMA	JMA	28.22	148.17	5351.89	2746	17.9	0.07	16.68	0.85
15	AOC ch4 surface event NOAA	NOAA	-2.76	-24.97	12.41	234	13.61	-1.06	8.39	0.38
16	ARH ch4 surface event NIWA	NIWA	-77.83	166.2	184	189	5	1.43	2.48	0.33
17	ASC ch4 surface event NOAA	NOAA	-7.97	-14.4	90	4316	8.42	-2.38	5.25	0.47
18	ASK ch4 surface event NOAA	NOAA	23.26	5.63	2715	1984	11.21	1.47	7.33	0.44
19	AZR ch4 surface event NOAA	NOAA	38.76	-27.29	24	1553	17.5	-0.65	13.8	0.62
20	AZV ch4 surface hourly NIES	NIES	54.71	73.03	160	10548	47.68	-17.33	36.02	0.7
21	BAL ch4 surface event NOAA	NOAA	55.42	16.97	28	2566	41.28	2.26	24.34	0.35
22	BAO ch4 surface event NOAA	NOAA	40.05	-105	1884	3066	65.84	-32.5	64.07	1.19
23	BCK ch4 surface hourly EC	EC	62.8	-115.92	220	76883	25.6	-3.57	13.75	0.31
24	BGI ch4 aircraft event NOAA	NOAA	42.82	-94.41	4221.49	355	18.64	1.97	17.54	1.02
25	BGU ch4 surface event LSCE	LSCE	41.97	3.23	13.67	536	25.07	-4.09	23.47	0.9
26	BHD ch4 surface event NIWA	NIWA	-41.41	174.87	85	311	6.68	1.77	4.43	0.51
27	BHD ch4 surface event NOAA	NOAA	-41.41	174.87	91.41	615	5.65	2.96	4.25	0.84
28	BIK ch4 surface event MPI-BGC	MPI-BGC	53.2	22.75	183	414	62.37	5.93	33.07	0.29
29	BIR ch4 surface hourly NILU	NILU	58.39	8.25	218	8317	18.88	3.71	14.1	0.6

30	BIS ch4 surface hourly LSCE	LSCE	44.38	-1.23	214	86947	20.91	-0.14	16.61	0.63
31	BKT ch4 surface event NOAA	NOAA	-0.2	100.32	875	1546	28.46	13	27.97	1.17
32	BKT ch4 surface hourly BMKG	BMKG	-0.2	100.32	896	39862	56.25	-6.43	53.35	0.91
33	BKT ch4 surface hourly EMPA	EMPA	-0.2	100.32	896.5	8061	66.56	-11.71	64.88	0.98
34	BLK ch4 surface hourly EC	EC	64.33	-96.01	61	19836	19.02	-5.45	8.34	0.27
35	BME ch4 surface event NOAA	NOAA	32.37	-64.65	17	777	17.21	-3.26	15.17	0.81
36	BMW ch4 surface event NOAA	NOAA	32.26	-64.88	56.26	1899	13.99	0.46	10.96	0.61
37	BNE ch4 aircraft event NOAA	NOAA	40.8	-97.18	3736.54	1098	20.14	3.58	21.66	0.95
38	BRA ch4 surface hourly EC	EC	50.2	-104.71	630	80974	45.49	1.58	28.65	0.4
39	BRW ch4 surface event NOAA	NOAA	71.32	-156.6	21.18	4803	17.08	1.31	12.55	0.55
40	BRW ch4 surface hourly NOAA	NOAA	71.32	-156.61	27.67	94835	19.54	2.12	16.42	0.72
41	BRZ ch4 surface hourly NIES	NIES	56.15	84.33	248	22219	41.2	3.14	33.7	0.67
42	BSC ch4 surface event NOAA	NOAA	44.18	28.66	5	1356	62.46	-4.66	57.24	0.84
43	BWD ch4 surface event NOAA	NOAA	38.93	-76.96	67.97	54	40.77	-15.38	31.07	0.71
44	CAR ch4 aircraft event NOAA	NOAA	40.79	-104.57	4788.81	8536	15.52	1.46	17.3	0.79
45	CBA ch4 surface event NOAA	NOAA	55.21	-162.72	41.62	4377	13.63	-6.49	10.58	0.85
46	CBW ch4 surface hourly ECN	ECN	51.97	4.93	200	47412	46.45	-14.42	41.88	0.91
47	CBY ch4 surface hourly EC	EC	69.13	-105.06	47	66185	13.64	-6.11	9.38	0.67
48	CDL ch4 surface hourly EC	EC	53.99	-105.12	630	31137	31.06	-1.68	20.47	0.44
49	CEA ch4 aircraft event NIES	NIES	62.11	78.35	10612.34	887	42.59	37.18	42.8	1.72
50	CFA ch4 surface event CSIRO	CSIRO	-19.28	147.06	5	745	5.77	-1.23	4.57	0.67
51	CGO ch4 surface event NOAA	NOAA	-40.68	144.68	164	1915	7.99	3.51	4.27	0.48
52	CHC ch4 surface hourly LSCE	LSCE	-16.2	-68.1	5355	49218	20.05	-11.53	18.72	1.2
53	CHL ch4 surface event EC	EC	58.75	-94.07	95	711	58.9	-0.58	26.22	0.2
54	CHL ch4 surface hourly EC	EC	58.74	-93.82	89	63471	52.29	-2.09	16.74	0.1
55	CHM ch4 surface hourly EC	EC	49.69	-74.34	423	23872	28.31	-2.39	11.35	0.17
56	CHR ch4 surface event NOAA	NOAA	1.7	-157.15	4.97	1423	13.42	-1.96	9.85	0.56
57	CHS ch4 surface hourly NOAA	NOAA	68.51	161.53	64.4	108724	21.98	-7.28	20.63	0.99
58	CIB ch4 surface event NOAA	NOAA	41.81	-4.93	849.99	1071	23.78	8.11	22.89	1.05
59	CMA ch4 aircraft event NOAA	NOAA	38.85	-74.31	3479.9	3273	20.39	4.19	17.13	0.74
60	CMN ch4 surface hourly IAFMS	IAFMS	44.17	10.68	2177	48861	19.07	-3.77	15.93	0.74
61	CMN ch4 surface hourly ICOS	ICOS	44.19	10.7	2173	22346	19.58	0.53	17.07	0.76
62	CMN ch4 surface hourly UNIURB	UNIURB	44.17	10.68	2172	10299	29.26	-3.56	28.51	0.96
63	CMO ch4 surface event NOAA	NOAA	45.48	-123.97	35	47	17.65	-0.84	14.57	0.67
64	COI ch4 surface hourly NIES	NIES	43.16	145.5	94	8714	21.9	-4.28	14.15	0.46

65	CON ch4 aircraft event NIES	NIES	4.08	142.67	11018.63	2400	15.34	-2.28	13.41	0.77
66	CPA ch4 surface hourly EMPA	EMPA	42.64	77.07	1623	30097	29.41	-6.24	22.51	0.63
67	CPS ch4 surface hourly EC	EC	49.82	-74.98	420.81	75148	30.87	-2.73	11.8	0.15
68	CPT ch4 surface event NOAA	NOAA	-34.35	18.49	260	746	5	3.18	3.68	0.95
69	CPT ch4 surface hourly SAWS	SAWS	-34.35	18.49	260	140642	5	0.98	4.53	0.86
70	CRI ch4 surface event CSIRO	CSIRO	15.08	73.83	66	212	40.82	0.65	32.93	0.65
71	CRV ch4 surface hourly NOAA	NOAA	64.99	-147.6	643.13	237517	15.54	2.21	13.06	0.73
72	CRZ ch4 surface event NOAA	NOAA	-46.43	51.85	202	1862	5.7	2.24	2.95	0.42
73	CVO ch4 surface event MPI-BGC	MPI-BGC	16.86	-24.87	10	661	10.52	2.91	6.96	0.51
74	CVO ch4 surface hourly UOE	UOE	16.86	-24.87	31	53706	11.42	3.52	7.69	0.55
75	CYA ch4 surface event CSIRO	CSIRO	-66.28	110.52	55	766	5	0.86	2.13	0.21
76	DEM ch4 surface hourly NIES	NIES	59.79	70.87	126	14115	52.84	-3.9	33.97	0.42
77	DEU ch4 surface hourly UBA	UBA	49.77	7.05	480	8442	38.65	-1.59	33.04	0.73
78	DND ch4 aircraft event NOAA	NOAA	47.81	-98.55	3747.55	2127	18.98	2.42	15.11	0.67
79	DRP ch4 surface event NOAA	NOAA	-59.16	-62.59	10	641	5	1.17	2.28	0.26
80	DSI ch4 surface event NOAA	NOAA	20.7	116.73	8	1062	28.08	-4.95	22.95	0.7
81	DWS ch4 surface hourly EC	EC	43.78	-79.47	218	90374	47.6	-7.17	32.33	0.48
82	EGB ch4 surface hourly EC	EC	44.23	-79.78	270.54	112225	41.85	1.02	26.67	0.41
83	EIC ch4 surface event NOAA	NOAA	-27.15	-109.44	60.96	1561	6.66	-2.26	3.51	0.41
84	ESP ch4 aircraft event NOAA	NOAA	49.41	-126.45	2746.03	5011	12.29	1.57	9.92	0.66
85	ESP ch4 surface event EC	EC	49.38	-126.55	79	1285	12.13	-2.26	9.3	0.62
86	ESP ch4 surface hourly EC	EC	49.38	-126.54	47	98212	12.92	-1.52	9.97	0.61
87	EST ch4 surface hourly EC	EC	51.67	-110.21	752.01	91009	69.52	-10.08	66.1	0.9
88	ETL ch4 aircraft event NOAA	NOAA	54.31	-104.94	3089.39	3220	21.6	2.12	13.37	0.44
89	ETL ch4 surface hourly EC	EC	54.35	-104.99	598	118445	33.76	0.04	19.42	0.33
90	FKL ch4 surface event LSCE	LSCE	35.34	25.67	151.41	347	28.71	10.48	17.45	0.5
91	FKL ch4 surface hourly LSCE	LSCE	35.34	25.67	165	55471	29.94	11.61	13.96	0.37
92	FNE ch4 surface hourly EC	EC	58.84	-122.57	376	49095	41.4	1.93	25.41	0.38
93	FSD ch4 surface hourly EC	EC	49.88	-81.57	250	151131	40.37	-2.25	14.53	0.13
94	FTL ch4 aircraft event NOAA	NOAA	-4.15	-38.28	2120.18	159	8.32	-1.68	8.49	1.03
95	FWI ch4 aircraft event NOAA	NOAA	44.7	-91.01	4212.13	379	20.13	0.72	19.27	0.69
96	GAT ch4 surface hourly ICOS	ICOS	53.07	11.44	224.86	186927	35.05	-0.53	26.27	0.55
97	GIF ch4 surface hourly LSCE	LSCE	48.71	2.15	167	50783	27.76	-1.6	23.89	0.74
98	GMI ch4 surface event NOAA	NOAA	13.39	144.66	6.33	3228	15.56	-0.02	11.63	0.53
99	GOZ ch4 surface event NOAA	NOAA	36.05	14.89	6	40	29.09	14.64	24.09	0.92

100	GPA ch4 surface event CSIRO	CSIRO	-12.25	131.04	37	107	20.87	-13.96	20.42	1.4
101	HAT ch4 surface hourly NIES	NIES	24.06	123.81	47.3	8771	21.67	-7.42	18.21	0.82
102	HBA ch4 surface event NOAA	NOAA	-75.61	-26.21	35	1896	6.26	1.83	2.72	0.27
103	HEL ch4 surface hourly ICOS	ICOS	54.18	7.88	153	1761	46.38	2.75	44.32	0.91
104	HFM ch4 aircraft event NOAA	NOAA	42.54	-72.17	3850.92	1676	18.58	1.67	14.3	0.67
105	HFM ch4 surface event NOAA	NOAA	42.54	-72.17	369	12	40	-4.38	10.78	0.08
106	HIL ch4 aircraft event NOAA	NOAA	40.04	-87.94	4157.22	3978	20.03	5.29	15.93	0.76
107	HLE ch4 surface event LSCE	LSCE	32.78	78.96	4522	268	33.85	31.58	20.67	1.24
108	HNP ch4 surface hourly EC	EC	43.61	-79.39	97	45698	46.98	-11.74	33.76	0.58
109	HPB ch4 surface event NOAA	NOAA	47.8	11.02	990	1549	49.79	1.18	40.48	0.66
110	HPB ch4 surface hourly DWD	DWD	47.8	11.02	1116	8640	47.45	-6.55	36.99	0.63
111	HPB ch4 surface hourly ICOS	ICOS	47.8	11.02	1027.94	133719	59.45	-1.78	38.97	0.43
112	HSU ch4 surface event NOAA	NOAA	41.05	-124.6	7.6	168	20.95	15.13	15.73	1.08
113	HTM ch4 surface hourly ICOS	ICOS	56.1	13.42	198.44	107785	34.83	0.16	16.65	0.23
114	HUN ch4 surface event NOAA	NOAA	46.95	16.65	344	2391	37.04	-7.78	32.7	0.82
115	HUN ch4 surface hourly ELTE	ELTE	46.95	16.65	344	33597	37.44	-9.17	32.06	0.79
116	ICE ch4 surface event NOAA	NOAA	63.4	-20.29	125.88	2323	16.51	-3.68	8.91	0.34
117	IGR ch4 surface hourly NIES	NIES	63.19	64.42	56	15135	72.94	-43.83	68.15	1.23
118	INU ch4 surface hourly EC	EC	68.32	-133.53	123	81970	18.69	-6.59	15.64	0.82
119	INX ch4 surface event NOAA	NOAA	39.58	-86.42	376.73	2297	41.56	1.5	25.85	0.39
120	IPR ch4 surface hourly ICOS	ICOS	45.81	8.63	289.94	91991	94.6	-45.3	80.08	0.92
121	IPR ch4 surface hourly IES	IES	45.81	8.63	239	57160	83.7	-30.84	72.15	0.88
122	ITN ch4 surface event NOAA	NOAA	35.37	-77.39	505	228	27.96	-8.33	22.8	0.75
123	IZO ch4 surface event NOAA	NOAA	28.3	-16.49	2377.9	2222	11.49	1.24	9.38	0.68
124	IZO ch4 surface hourly AEMET	AEMET	28.31	-16.5	2398.2	161589	12.63	1.62	11.23	0.8
125	JFJ ch4 surface event MPI-BGC	MPI-BGC	46.55	7.99	3570	327	15.98	2.38	11.47	0.54
126	JFJ ch4 surface hourly EMPA	EMPA	46.55	7.99	3580	122515	18.32	-0.68	15.21	0.69
127	JFJ ch4 surface hourly ICOS	ICOS	46.55	7.99	3575	36049	16.5	1.91	13.02	0.64
128	JGS ch4 surface hourly KMA	KMA	33.3	126.16	71.47	64134	38.83	-8.46	31.64	0.71
129	KAS ch4 surface hourly AGH	AGH	49.23	19.98	1991	24643	27.16	-1.43	19.69	0.53
130	KCO ch4 surface event NOAA	NOAA	4.97	73.47	6	89	19.26	-3.52	9.84	0.29
131	KEY ch4 surface event NOAA	NOAA	25.67	-80.18	6	1845	18.75	3.99	16.4	0.81
132	KIT ch4 surface hourly ICOS	ICOS	49.09	8.42	208.75	155325	31.53	-4.27	27.62	0.77
133	KJO ch4 surface event MPI-BGC	MPI-BGC	70.85	29.24	5	175	21.46	-3.34	12.44	0.36
134	KMP ch4 surface hourly FMI	FMI	60.2	24.96	56	64423	44.98	-1.4	17.27	0.15
135	KRE ch4 surface hourly ICOS	ICOS	49.58	15.08	645.47	122130	31.7	-1.73	23.52	0.54

136	KRS ch4 surface hourly NIES	NIES	58.25	82.42	143	13974	36.26	-14.2	26.05	0.67
137	KUM ch4 surface event NOAA	NOAA	19.53	-154.83	8.78	4857	10.77	3.37	7.84	0.63
138	KZD ch4 surface event NOAA	NOAA	44.31	76.07	484.82	1105	31.24	-8.96	27.13	0.81
139	KZM ch4 surface event NOAA	NOAA	43.25	77.87	2524	1110	21.33	-1.15	18.7	0.77
140	LAU ch4 surface event NIWA	NIWA	-45.03	169.67	380	419	8.41	0.19	6.9	0.67
141	LEF ch4 aircraft event NOAA	NOAA	45.96	-90.19	2124.24	4789	35.82	2.91	17.03	0.27
142	LEF ch4 surface event NOAA	NOAA	45.94	-90.27	842.99	4412	58.68	3.32	23.26	0.16
143	LEF ch4 surface hourly NOAA	NOAA	45.95	-90.27	868	235783	58.39	0.91	21.6	0.14
144	LEW ch4 surface event NOAA	NOAA	40.94	-76.88	261	850	50.95	-16.26	38.57	0.67
145	LIN ch4 surface hourly ICOS	ICOS	52.17	14.12	111.43	191222	33.47	-0.09	24.34	0.53
146	LLB ch4 surface event NOAA	NOAA	54.95	-112.45	568.25	418	88.61	-5.32	61.38	0.44
147	LLB ch4 surface hourly EC	EC	54.95	-112.47	584.37	102918	58.11	-1.95	57.05	0.77
148	LLN ch4 surface event NOAA	NOAA	23.47	120.87	2867	1576	22.37	-3.03	17.55	0.63
149	LMP ch4 surface event NOAA	NOAA	35.52	12.62	50	1345	21.05	11	15.55	0.82
150	LMP ch4 surface hourly ICOS	ICOS	35.52	12.63	53	12584	22.49	5.9	13.99	0.46
151	LPO ch4 surface event LSCE	LSCE	48.8	-3.58	20	241	29.97	-0.56	27.8	0.86
152	LUT ch4 surface hourly ICOS	ICOS	53.4	6.35	61	20378	61.47	-9.8	52.38	0.75
153	MAA ch4 surface event CSIRO	CSIRO	-67.62	62.87	42	860	5	0.83	2.08	0.2
154	MAN ch4 aircraft event INPE	INPE	-2.49	-59.82	2655.44	2849	16.31	-0.15	12.34	0.56
155	MBC ch4 surface event NOAA	NOAA	76.25	-119.35	35	54	8.38	-0.26	8.91	1.11
156	MBO ch4 surface event NOAA	NOAA	43.98	-121.69	2742.3	1914	15.17	0.39	13.11	0.75
157	MDM ch4 surface event ENEA	ENEA	37.88	14.03	1653	395	21.05	-9.34	18.03	0.93
158	MEX ch4 surface event NOAA	NOAA	18.98	-97.31	4469	967	14.18	0.58	11.42	0.65
159	MHD ch4 surface event LSCE	LSCE	53.33	-9.9	29.24	580	15.06	3.31	10.55	0.54
160	MHD ch4 surface event NOAA	NOAA	53.33	-9.9	26.1	2037	16.32	0.45	9.82	0.36
161	MHD ch4 surface hourly LSCE	LSCE	53.33	-9.9	29	24117	14.64	2.44	6.44	0.22
162	MID ch4 surface event NOAA	NOAA	28.21	-177.37	10.42	2392	11.11	-0.75	9.14	0.68
163	MKN ch4 surface event NOAA	NOAA	-0.06	37.3	3649	309	18.33	-7.97	12.47	0.65
164	MLO ch4 surface event NOAA	NOAA	19.53	-155.58	3419.6	5201	11.04	4.1	8.2	0.69
165	MLO ch4 surface hourly NOAA	NOAA	19.54	-155.58	3437	61011	11.93	2.89	9.41	0.68
166	MNM ch4 surface hourly JMA	JMA	24.29	153.98	27.1	168068	12.53	1.87	10.49	0.72
167	MQA ch4 surface event CSIRO	CSIRO	-54.48	158.97	13	923	5	0.66	2.79	0.33
168	MSH ch4 surface event NOAA	NOAA	41.66	-70.5	78.3	515	30.39	-0.4	23.38	0.59
169	MVY ch4 surface event NOAA	NOAA	41.33	-70.57	16	210	26.47	0.22	21.97	0.69
170	MWO ch4 surface event NOAA	NOAA	34.22	-118.06	1775.23	4441	40.13	-19.28	39.5	1.2
171	NAT ch4 surface event NOAA	NOAA	-5.64	-35.23	49.96	747	9.68	-2.18	8.34	0.79

172	NGL ch4 surface hourly UBA	UBA	53.17	13.03	71.4	8717	32.57	2	26.05	0.64
173	NHA ch4 aircraft event NOAA	NOAA	42.92	-70.56	3159.38	4256	19.6	3.83	13.52	0.56
174	NMB ch4 surface event MPI-BGC	MPI-BGC	-23.58	15.03	456	282	9.15	-0.53	8.07	0.78
175	NMB ch4 surface event NOAA	NOAA	-23.58	15.03	461	1344	10.09	0.37	7.91	0.62
176	NOR ch4 surface hourly ICOS	ICOS	60.09	17.48	109.2	113340	35.12	-0.27	11.84	0.11
177	NOV ch4 aircraft event NIES	NIES	55	83	3059.76	3094	28.07	6.5	21.24	0.61
178	NOY ch4 surface hourly NIES	NIES	63.43	75.78	151	13575	61.96	-27.65	49.43	0.84
179	NSK ch4 aircraft event NOAA	NOAA	58.8	-104.6	2913.52	45	11.52	0.25	11.12	0.83
180	NWP ch4 surface event TU	TU	-4.09	152.2	20	3600	25.23	-4.24	19.03	0.6
181	NWR ch4 surface event NOAA	NOAA	40.05	-105.58	3526.12	6285	16.79	1.19	14.95	0.76
182	NYA ch4 surface event TU	TU	78.92	11.93	43	926	15.45	1.6	10.74	0.49
183	OBN ch4 surface event NOAA	NOAA	55.1	36.6	484	451	56.81	-17.58	49.76	0.86
184	OHP ch4 surface hourly LSCE	LSCE	43.92	5.75	637.38	54626	27.85	9.48	16.59	0.47
185	OIL ch4 aircraft event NOAA	NOAA	41.28	-88.94	4228.96	424	18.43	3.01	15.03	0.8
186	OPE ch4 surface hourly ICOS	ICOS	48.56	5.5	450.8	124659	27.66	1.45	21.62	0.61
187	ORL ch4 aircraft event LSCE	LSCE	47.83	2.5	1332.2	1937	26.04	8.17	24.03	0.96
188	OXK ch4 surface event MPI-BGC	MPI-BGC	50.03	11.81	1022	596	24.16	-0.06	20.7	0.73
189	OXK ch4 surface event NOAA	NOAA	50.03	11.81	1181.3	1203	32.96	-9.5	29.99	0.88
190	OXK ch4 surface hourly ICOS	ICOS	50.03	11.81	1114.01	47602	29.45	-11.76	24.86	0.84
191	PAL ch4 surface event NOAA	NOAA	67.97	24.12	570	1739	29.67	-5.51	13.5	0.24
192	PAL ch4 surface hourly FMI	FMI	67.97	24.12	567	131491	27.59	-5.75	13.05	0.27
193	PAL ch4 surface hourly ICOS	ICOS	67.97	24.12	577	33955	29.31	-5.73	11.86	0.2
194	PCO ch4 surface event NOAA	NOAA	38.47	-28.4	2230	12	29.01	13.87	12.12	0.39
195	PDI ch4 surface hourly EMPA	EMPA	21.57	103.52	1478	7037	46.13	-7.14	36.51	0.65
196	PDI ch4 surface hourly VNMHA	VNMHA	21.57	103.52	1478	40926	46.65	-21.24	40.08	0.95
197	PDM ch4 surface event LSCE	LSCE	42.94	0.14	2879.63	422	20.83	-0.73	19.59	0.87
198	PDM ch4 surface hourly LSCE	LSCE	42.94	0.14	2887	29118	14.16	1.81	10.29	0.54
199	PFA ch4 aircraft event NOAA	NOAA	64.98	-148.12	3578.54	4942	13.67	0.98	10.97	0.59
200	PIP ch4 aircraft event TU	TU	37.81	141.35	1911.49	2044	27.21	-0.11	25.41	0.82
201	POC ch4 surface event NIWA	NIWA	0.99	126.45	25.85	350	18.78	4.4	11.96	0.46
202	POC ch4 surface event NOAA	NOAA	-1.31	-114.59	20	7298	19.11	-1.6	10.24	0.29
203	PRS ch4 surface hourly RSE	RSE	45.94	7.71	3490	77559	21.5	9.81	17.82	0.9
204	PSA ch4 surface event NOAA	NOAA	-64.77	-64.05	15	2386	5.82	1.29	2.45	0.23
205	PTA ch4 surface event NOAA	NOAA	38.95	-123.73	22	947	28.51	9.2	28.51	1.1
206	PUY ch4 surface event LSCE	LSCE	45.77	2.97	1469.32	650	21.26	-7.72	18.64	0.91
207	PUY ch4 surface hourly ICOS	ICOS	45.77	2.97	1475	42227	18.72	-10.53	14.99	0.96

208	PUY ch4 surface hourly LSCE	LSCE	45.77	2.97	1475	49795	19.65	-10.6	15.71	0.93
209	RBA ch4 aircraft event INPE	INPE	-9.2	-66.35	2320.43	2266	17.3	-5.82	18.9	1.23
210	RGL ch4 surface hourly UNIVBRIS	UNIVBRIS	52	-2.54	273.96	73326	28.96	-5.14	23.69	0.68
211	RPB ch4 surface event NOAA	NOAA	13.16	-59.43	20	2388	12.03	2.33	7.97	0.48
212	RTA ch4 aircraft event NOAA	NOAA	-21.24	-159.8	3178.36	3262	6.7	-4.87	5.31	1.12
213	RUN ch4 surface hourly ICOS	ICOS	-21.08	55.38	2160	25300	5	-2.46	4.36	1
214	RYO ch4 surface hourly JMA	JMA	39.03	141.82	280	170510	24.19	-1.65	17.28	0.51
215	SAC ch4 surface hourly ICOS	ICOS	48.72	2.14	221.47	91926	30.05	-1.45	24.62	0.66
216	SAN ch4 aircraft event INPE	INPE	-2.85	-54.96	2118.78	2387	25.27	-13.16	28.33	1
217	SAN ch4 aircraft event NOAA	NOAA	-2.86	-54.86	1979.62	333	25.84	-19.57	28.8	1.43
218	SCA ch4 aircraft event NOAA	NOAA	32.85	-79.5	4133.68	3844	17.62	6.03	15.62	0.86
219	SCS ch4 surface event NOAA	NOAA	11.88	110.41	20	678	24.42	3.43	23.34	0.93
220	SCT ch4 surface event NOAA	NOAA	33.41	-81.83	420	3334	32.62	-4.9	27.73	0.74
221	SCT ch4 surface hourly NOAA	NOAA	33.41	-81.83	420.2	145029	29.77	-2.4	25.45	0.74
222	SDZ ch4 surface event NOAA	NOAA	40.65	117.12	298	584	62.62	-18.92	65.52	1.18
223	SEY ch4 surface event NOAA	NOAA	-4.68	55.53	7	2201	14.43	-1.97	8.77	0.39
224	SGP ch4 aircraft event NOAA	NOAA	36.63	-97.51	2299.24	7722	33.52	-5.03	31.19	0.7
225	SGP ch4 surface event NOAA	NOAA	36.67	-97.49	374	2461	57.81	-25.7	48.81	0.91
226	SHM ch4 surface event NOAA	NOAA	52.72	174.11	28	2334	15.51	-2.42	10.62	0.49
227	SIS ch4 surface event CSIRO	CSIRO	60.09	-1.25	33	103	16.81	3.91	12.26	0.58
228	SIS ch4 surface event MPI-BGC	MPI-BGC	60.09	-1.25	30	850	23.81	6.19	16.19	0.53
229	SMO ch4 surface event NOAA	NOAA	-14.25	-170.57	53.52	4457	7.48	-3.13	5.16	0.65
230	SMR ch4 surface hourly ICOS	ICOS	61.85	24.29	250.18	118630	41.75	2.44	12.78	0.1
231	SOD ch4 surface hourly FMI	FMI	67.36	26.64	227	45822	35.74	-6.65	15.62	0.23
232	SPO ch4 surface event NOAA	NOAA	-89.98	-24.8	2817.19	3589	5.87	1.15	3.08	0.31
233	SSL ch4 surface hourly UBA	UBA	47.92	7.92	1217	8273	22.36	-0.54	19.92	0.79
234	STE ch4 surface hourly ICOS	ICOS	53.04	8.46	164.66	88652	56.81	-11.39	49.48	0.77
235	STM ch4 surface event NOAA	NOAA	66	2	6.17	2344	19.26	-0.76	12.09	0.39
236	STR ch4 surface event NOAA	NOAA	37.76	-122.45	486	6800	40.97	14.89	38.71	1.02
237	SUM ch4 surface event NOAA	NOAA	72.6	-38.42	3214.54	2136	13.43	-1.05	7.49	0.32
238	SUR ch4 aircraft event NIES	NIES	61.2	73.2	2907.9	3062	31.41	2.53	26.92	0.64
239	SVB ch4 surface hourly ICOS	ICOS	64.26	19.77	324.62	105509	35.37	-0.69	11.12	0.1
240	SVV ch4 surface hourly NIES	NIES	51.33	82.13	534.37	11085	120.75	-187.87	111.85	3.28
241	SYO ch4 surface event NOAA	NOAA	-69	39.58	17.06	1143	6.14	1.51	2.58	0.24
242	TAB ch4 aircraft event INPE	INPE	-5.64	-69.85	2236.73	464	22.02	-15.57	22.65	1.41

243	TAC ch4 surface event NOAA	NOAA	52.52	1.14	236	103	41.57	3.25	15.43	0.14
244	TAC ch4 surface hourly UNIVBRIS	UNIVBRIS	52.52	1.14	176.09	68199	35.78	7.56	27.71	0.62
245	TAO ch4 surface hourly EC	EC	43.66	-79.4	100	16708	47.43	-17.24	31.4	0.57
246	TAP ch4 surface event NOAA	NOAA	36.73	126.13	21	3324	42.35	-0.8	29.7	0.49
247	TDA ch4 aircraft event TU	TU	36.02	135.65	7084.95	2690	30.77	-7	28.85	0.92
248	TEF ch4 aircraft event INPE	INPE	-3.48	-66.04	2172.76	646	22.7	-9.41	24.63	0.81
249	TER ch4 surface event MGO	MGO	69.2	35.1	42	918	23.84	-12.33	17.96	0.83
250	TGC ch4 aircraft event NOAA	NOAA	27.69	-96.75	3934.71	2984	18.64	3.06	18.33	0.78
251	THD ch4 aircraft event NOAA	NOAA	41.09	-124.22	3849.95	2734	17.88	3.81	18.66	0.92
252	THD ch4 surface event NOAA	NOAA	41.05	-124.15	112	1505	19.78	1.13	14.82	0.56
253	TIK ch4 surface event MGO	MGO	71.59	128.92	18	241	27.17	-3.32	25.92	0.92
254	TIK ch4 surface event NOAA	NOAA	71.6	128.89	29	652	21.84	-1.29	19.97	0.84
255	TIK ch4 surface hourly FMI	FMI	71.6	128.89	29	75491	21.94	-1.86	20.85	0.91
256	TLL ch4 surface hourly DMC	DMC	-30.17	-70.8	2159	48055	15.19	-1.93	8.99	0.37
257	TLL ch4 surface hourly EMPA	EMPA	-30.17	-70.8	2225	7406	9.79	-2.36	5.47	0.37
258	TMD ch4 surface event NOAA	NOAA	39.58	-77.49	673.91	141	41.37	-12.36	35.73	0.83
259	TOH ch4 surface hourly ICOS	ICOS	51.81	10.53	886.74	125927	29.23	-0.82	22.01	0.57
260	TPD ch4 surface hourly EC	EC	42.64	-80.56	266	67411	43.03	4.33	29.37	0.48
261	TRM ch4 surface event LSCE	LSCE	-15.88	54.52	10	105	9.71	2.8	11.08	1.37
262	TRN ch4 surface hourly ICOS	ICOS	47.96	2.11	214.7	143295	29.21	0.73	23.54	0.64
263	TRN ch4 surface hourly LSCE	LSCE	47.96	2.11	311	27395	26.7	0.54	22.39	0.7
264	TTA ch4 surface hourly UOB	UOB	56.56	-2.99	622	40878	19.94	-6.36	16.12	0.75
265	ULB ch4 aircraft event NOAA	NOAA	47.4	106.04	2713.23	552	17.43	1.63	11.11	0.41
266	ULD ch4 surface hourly KMA	KMA	37.48	130.9	220.9	54305	37.34	-5.76	29.58	0.65
267	USH ch4 surface event NOAA	NOAA	-54.85	-68.31	32	1374	5	1.35	2.37	0.3
268	UTA ch4 surface event NOAA	NOAA	39.9	-113.72	1332	2460	21	0.63	17.16	0.67
269	UTO ch4 surface hourly FMI	FMI	59.78	21.37	64	43561	43.17	2.89	13.62	0.1
270	UTO ch4 surface hourly ICOS	ICOS	59.78	21.37	65	28781	47.65	2.11	12.33	0.07
271	UUM ch4 surface event NOAA	NOAA	44.45	111.1	1012	2266	27.86	1.4	19.5	0.49
272	VGN ch4 surface hourly NIES	NIES	54.5	62.32	277	15037	29.39	-4.85	25.69	0.79
273	VKV ch4 surface hourly MGO	MGO	59.95	30.7	76	25870	76.57	-17.53	47.52	0.44
274	WBI ch4 aircraft event NOAA	NOAA	41.85	-91.44	4177.05	3474	21.11	4.29	17.19	0.75
275	WBI ch4 surface event NOAA	NOAA	41.72	-91.35	620.6	3814	43.29	-5.03	29.66	0.48
276	WGC ch4 aircraft event NOAA	NOAA	38.18	-119.8	901.79	165	29.07	-8.85	30.66	1.12

277	WGC ch4 surface event NOAA	NOAA	38.26	-121.49	93.39	2933	120.92	-49.03	115.76	1.08
278	WGC ch4 surface hourly NOAA	NOAA	38.26	-121.49	285.25	343102	89.43	-22.5	95.57	1.04
279	WIS ch4 surface event NOAA	NOAA	30.64	34.85	401.92	2361	25.06	2.65	19.25	0.61
280	WKT ch4 surface event NOAA	NOAA	31.31	-97.33	617.72	4060	47.39	-10.16	44.62	0.93
281	WLG ch4 surface event NOAA	NOAA	36.28	100.9	3823.87	2418	15.28	-0.96	11.77	0.6
282	WPC ch4 surface event NOAA	NOAA	0.79	151.25	10	552	14.59	-1.68	8.81	0.38
283	WSA ch4 surface event EC	EC	43.93	-60.02	30	1182	19.78	-2.98	14.16	0.53
284	WSA ch4 surface hourly EC	EC	43.93	-60.01	30	98715	18.07	-2.55	12.03	0.46
285	YAK ch4 surface hourly NIES	NIES	62.09	129.36	341	10654	27.94	-7.07	20.43	0.6
286	YON ch4 surface hourly JMA	JMA	24.47	123.01	50	168060	24.97	-3.73	20.84	0.72
287	ZEP ch4 surface event NOAA	NOAA	78.91	11.89	479	2528	16.16	2.98	10.56	0.46
288	ZEP ch4 surface hourly ICOS	ICOS	78.91	11.89	489	31923	16.87	4.39	9.56	0.39
289	ZEP ch4 surface hourly NILU	NILU	78.91	11.89	489	68159	32.58	3.4	30.85	0.91
290	ZGT ch4 surface hourly UBA	UBA	54.43	12.73	7.5	8360	36.14	-9.43	31.85	0.84
291	ZSF ch4 surface hourly UBA	UBA	47.42	10.98	2670	8287	27.1	-11.62	21.99	0.84
292	ZSF ch4 surface hourly UBAG	UBAG	47.42	10.98	2670	148212	21	3.25	16.67	0.65

Unassimilated

	Site Code	**Laboratory**	**Latitude**	**Longitude**	**Elevation (MASL)**	**No. of Observation**	**Model-data mismatch**	**Mean bias**	**Standard deviation of bias**	**Chi-squared**
1	AAO ch4 aircraft event NOAA	NOAA	40.14	-88.58	1966.82	3271	N/A	5.86	19.35	N/A
2	ABT ch4 surface hourly EC	EC	49.01	-122.34	93	51389	N/A	-114.93	117.05	N/A
3	ACG ch4 aircraft event NOAA	NOAA	67.81	-154.92	3129	1765	N/A	3.21	15.5	N/A
4	ACT ch4 aircraft event NOAA	NOAA	37.52	-87.69	2195.32	1486	N/A	-4.22	30.15	N/A
5	ALT ch4 surface event MPI-BGC	MPI-BGC	82.45	-62.51	185	432	N/A	-1.39	0	N/A
6	ALT ch4 surface hourly EC	EC	82.45	-62.51	195	150696	N/A	3.28	9.71	N/A
7	AMS ch4 surface hourly LSCE	LSCE	-37.8	77.54	75	12761	N/A	1.53	2.19	N/A
8	AMY ch4 surface hourly KMA	KMA	36.54	126.33	47	148695	N/A	-18.85	95.83	N/A
9	AZV ch4 surface hourly NIES	NIES	54.71	73.03	147.62	10548	N/A	-19.93	49.15	N/A
10	BAO ch4 aircraft event NOAA	NOAA	40.05	-105.01	3094.69	12	N/A	-26.3	49.2	N/A
11	BAO ch4 surface hourly NOAA	NOAA	40.05	-105	1719.16	4178	N/A	-49.27	73.25	N/A
12	BCK ch4 surface hourly EC	EC	62.8	-115.92	220	76883	N/A	-5.98	24.73	N/A
13	BIK ch4 surface event MPI-BGC	MPI-BGC	53.2	22.75	183	414	N/A	37.54	26.92	N/A
14	BIR ch4 surface hourly NILU	NILU	58.39	8.25	218	8317	N/A	-1.88	21.08	N/A

15	BIS ch4 surface hourly LSCE	LSCE	44.38	-1.23	214	86947	N/A	2.16	19.4	N/A
16	BKT ch4 surface hourly BMKG	BMKG	-0.2	100.32	896	39862	N/A	3.71	39.76	N/A
17	BKT ch4 surface hourly EMPA	EMPA	-0.2	100.32	896.5	8061	N/A	5.44	41.45	N/A
18	BLK ch4 surface hourly EC	EC	64.33	-96.01	61	19836	N/A	-8.14	11.53	N/A
19	BRA ch4 surface hourly EC	EC	50.2	-104.71	630	80974	N/A	-1.12	39.57	N/A
20	BRW ch4 surface hourly NOAA	NOAA	71.32	-156.61	27.69	94835	N/A	2.84	16.55	N/A
21	BRZ ch4 surface hourly NIES	NIES	56.15	84.33	200.48	22219	N/A	22.18	51.19	N/A
22	CAR ch4 aircraft event NOAA	NOAA	40.9	-104.8	5059.95	8536	N/A	4.39	13.28	N/A
23	CBW ch4 surface hourly ECN	ECN	51.97	4.93	82.54	47412	N/A	-63.36	133.75	N/A
24	CBY ch4 surface hourly EC	EC	69.13	-105.06	47	66185	N/A	-7.98	12.31	N/A
25	CDL ch4 surface hourly EC	EC	53.99	-105.12	630	31137	N/A	-6.09	29.25	N/A
26	CGO ch4 surface highfreq AGAGE	AGAGE	-40.68	144.69	151.92	183484	N/A	6.65	10.28	N/A
27	CHC ch4 surface hourly LSCE	LSCE	-16.2	-68.1	5355	49218	N/A	-7.01	15.33	N/A
28	CHL ch4 surface hourly EC	EC	58.74	-93.82	89	63471	N/A	-2.61	21.86	N/A
29	CHM ch4 surface hourly EC	EC	49.69	-74.34	423	23872	N/A	-2.45	15	N/A
30	CHS ch4 surface hourly NOAA	NOAA	68.51	161.53	46.19	108724	N/A	-12.95	33.98	N/A
31	CMN ch4 surface hourly IAFMS	IAFMS	44.17	10.68	2177	48861	N/A	-7.55	18.95	N/A
32	CMN ch4 surface hourly ICOS	ICOS	44.19	10.7	2173	22346	N/A	-3.71	22.3	N/A
33	CMN ch4 surface hourly UNIURB	UNIURB	44.17	10.68	2172	10299	N/A	-12.05	38.71	N/A
34	COB ch4 aircraft event NOAA	NOAA	42	-88.47	3172.08	640	N/A	-2.55	24.61	N/A
35	COI ch4 surface hourly NIES	NIES	43.16	145.5	94	8714	N/A	-6.18	16.99	N/A
36	CPA ch4 surface hourly EMPA	EMPA	42.64	77.07	1623	30097	N/A	-15.48	29.42	N/A
37	CPS ch4 surface hourly EC	EC	49.82	-74.98	420.99	75148	N/A	-3.15	14.31	N/A
38	CPT ch4 surface hourly SAWS	SAWS	-34.35	18.49	260	140642	N/A	4.83	5.89	N/A
39	CRV ch4 aircraft event NOAA	NOAA	64.4	-149.68	1446.07	2451	N/A	-12.38	51.41	N/A
40	CRV ch4 surface event NOAA	NOAA	64.99	-147.6	643.13	1648	N/A	0.46	14.63	N/A
41	CRV ch4 surface hourly NOAA	NOAA	64.99	-147.6	628.18	237517	N/A	2.87	15.17	N/A
42	CVO ch4 surface event MPI-BGC	MPI-BGC	16.86	-24.87	10	661	N/A	10.43	0	N/A
43	CVO ch4 surface hourly UOE	UOE	16.86	-24.87	31	53706	N/A	3.08	7.95	N/A
44	DEM ch4 surface hourly NIES	NIES	59.79	70.87	115.55	14115	N/A	-11.82	103.41	N/A
45	DEU ch4 surface hourly UBA	UBA	49.77	7.05	480	8442	N/A	-7.77	43.76	N/A
46	DWS ch4 surface hourly EC	EC	43.78	-79.47	218	90374	N/A	-28.5	74.88	N/A
47	EGB ch4 surface hourly EC	EC	44.23	-79.78	270.55	112225	N/A	-4.64	39.03	N/A
48	ESP ch4 surface hourly EC	EC	49.38	-126.54	47	98212	N/A	-1.13	10.71	N/A

49	EST ch4 surface hourly EC	EC	51.67	-110.21	752.2	91009	N/A	-35.11	109.8	N/A
50	ETL ch4 surface hourly EC	EC	54.35	-104.99	598	118445	N/A	-3.72	28.04	N/A
51	FAM ch4 aircraft event NOAA	NOAA	52.56	0.82	715.5	22	N/A	0.44	34.07	N/A
52	FKL ch4 surface hourly LSCE	LSCE	35.34	25.67	165	55471	N/A	10.55	13.83	N/A
53	FNE ch4 surface hourly EC	EC	58.84	-122.57	376	49095	N/A	8.31	39.52	N/A
54	FSD ch4 surface hourly EC	EC	49.88	-81.57	250	151131	N/A	-1.01	21.1	N/A
55	GAT ch4 surface hourly ICOS	ICOS	53.07	11.44	225.63	186927	N/A	5.79	32.43	N/A
56	GIF ch4 surface hourly LSCE	LSCE	48.71	2.15	167	50783	N/A	-1.76	40.31	N/A
57	GSN ch4 surface hourly NIER	NIER	33.15	126.12	144	7576	N/A	44.52	66.03	N/A
58	GVN ch4 surface event MPI-BGC	MPI-BGC	-70.67	-8.27	40	165	N/A	2.45	2.17	N/A
59	HAA ch4 aircraft event NOAA	NOAA	21.23	-158.91	3977.4	2343	N/A	0.41	9.69	N/A
60	HAT ch4 surface hourly NIES	NIES	24.06	123.81	47.3	8771	N/A	-7.47	18.14	N/A
61	HEL ch4 surface hourly ICOS	ICOS	54.18	7.88	153	1761	N/A	7.24	47.24	N/A
62	HIP ch4 aircraft event NOAA	NOAA	14.03	-91.36	5292.98	1384	N/A	3.66	19.1	N/A
63	HNP ch4 surface hourly EC	EC	43.61	-79.39	97	45698	N/A	-16.04	57.71	N/A
64	HOW ch4 aircraft event NOAA	NOAA	42.2	-68.13	1421.03	29	N/A	4.33	16.7	N/A
65	HPB ch4 surface hourly DWD	DWD	47.8	11.02	1107	8640	N/A	13.6	39.03	N/A
66	HPB ch4 surface hourly ICOS	ICOS	47.8	11.02	1027.3	133719	N/A	20.26	43.65	N/A
67	HTM ch4 surface hourly ICOS	ICOS	56.1	13.42	198.4	107785	N/A	-1.98	19.23	N/A
68	HUN ch4 surface hourly ELTE	ELTE	46.95	16.65	344	33597	N/A	2.8	39.67	N/A
69	IGR ch4 surface hourly NIES	NIES	63.19	64.42	42.65	15135	N/A	-78.6	116.25	N/A
70	INU ch4 surface hourly EC	EC	68.32	-133.53	123	81970	N/A	-7.48	20.39	N/A
71	INX ch4 aircraft event NOAA	NOAA	39.87	-86.2	1006.47	350	N/A	-4	25.82	N/A
72	INX ch4 surface event NOAA	NOAA	39.82	-86.03	352.16	2297	N/A	-19.28	131.96	N/A
73	IPR ch4 surface hourly ICOS	ICOS	45.81	8.63	290.08	91991	N/A	-41.01	100.04	N/A
74	IPR ch4 surface hourly IES	IES	45.81	8.63	239	57160	N/A	-48.75	109.38	N/A
75	IZO ch4 surface hourly AEMET	AEMET	28.31	-16.5	2397.55	161589	N/A	0.33	11.54	N/A
76	JFJ ch4 surface event MPI-BGC	MPI-BGC	46.55	7.99	3570	327	N/A	17.21	0	N/A
77	JFJ ch4 surface hourly EMPA	EMPA	46.55	7.99	3580	122515	N/A	-1.55	16.9	N/A
78	JFJ ch4 surface hourly ICOS	ICOS	46.55	7.99	3575	36049	N/A	0.91	14.74	N/A
79	JGS ch4 surface hourly KMA	KMA	33.3	126.16	71.47	64134	N/A	-17.08	38.54	N/A
80	KAS ch4 surface hourly AGH	AGH	49.23	19.98	1991	24643	N/A	-3.29	23.93	N/A
81	KIT ch4 surface hourly ICOS	ICOS	49.09	8.42	207.44	155325	N/A	5.08	39.51	N/A

82	KMP ch4 surface hourly FMI	FMI	60.2	24.96	56	64423	N/A	-3.85	26.64	N/A
83	KRE ch4 surface hourly ICOS	ICOS	49.58	15.08	645.88	122130	N/A	-11.13	40.16	N/A
84	KRS ch4 surface hourly NIES	NIES	58.25	82.42	125.24	13974	N/A	-16.47	37.61	N/A
85	LAC ch4 surface event NOAA	NOAA	34.07	-118.21	230	839	N/A	-52.21	89.64	N/A
86	LAU ch4 surface hourly NIWA	NIWA	-45.04	169.68	380	1187	N/A	1.64	6.81	N/A
87	LEF ch4 aircraft event NOAA	NOAA	45.93	-90.27	2536.44	4789	N/A	7.79	26.79	N/A
88	LEF ch4 surface hourly NOAA	NOAA	45.95	-90.27	635.89	235783	N/A	1.89	27.16	N/A
89	LIN ch4 surface hourly ICOS	ICOS	52.17	14.12	111.04	191222	N/A	-3.72	44.38	N/A
90	LLB ch4 surface hourly EC	EC	54.95	-112.47	584.57	102918	N/A	-12.18	83.55	N/A
91	LMP ch4 surface event ENEA	ENEA	35.52	12.63	47	1031	N/A	11.71	19.61	N/A
92	LMP ch4 surface hourly ENEA	ENEA	35.52	12.63	47	1042	N/A	11.3	27.5	N/A
93	LMP ch4 surface hourly ICOS	ICOS	35.52	12.63	53	12584	N/A	8.89	14.33	N/A
94	LUT ch4 surface hourly ICOS	ICOS	53.4	6.35	61	20378	N/A	-31.44	87.55	N/A
95	MCI ch4 aircraft event NOAA	NOAA	41.05	-89.88	1247.36	128	N/A	-10.23	19.38	N/A
96	MHD ch4 surface highfreq AGAGE	AGAGE	53.33	-9.9	25	9765	N/A	0.61	12.58	N/A
97	MHD ch4 surface hourly LSCE	LSCE	53.33	-9.9	29	24117	N/A	3.57	6.96	N/A
98	MLO ch4 surface hourly NOAA	NOAA	19.54	-155.58	3437	61011	N/A	1.67	11.15	N/A
99	MNM ch4 surface hourly JMA	JMA	24.29	153.98	27.1	168068	N/A	2.04	10.43	N/A
100	MRC ch4 aircraft event NOAA	NOAA	41.7	-76.22	1264.79	77	N/A	-8.83	13.94	N/A
101	MRC ch4 surface event NOAA	NOAA	41.53	-76.27	622.87	874	N/A	-12.31	54.06	N/A
102	NEB ch4 surface event NOAA	NOAA	39.32	-76.58	110.95	82	N/A	-29.15	49.01	N/A
103	NGL ch4 surface hourly UBA	UBA	53.17	13.03	71.4	8717	N/A	10.04	36.14	N/A
104	NGM ch4 surface event TU	TU	-1.85	149.81	20	629	N/A	-6.1	38.82	N/A
105	NOR ch4 surface hourly ICOS	ICOS	60.09	17.48	109.33	113340	N/A	-1.38	13.92	N/A
106	NOY ch4 surface hourly NIES	NIES	63.43	75.78	138.35	13575	N/A	-42.96	96.75	N/A
107	NSA ch4 aircraft event NOAA	NOAA	69	-151.06	1467.96	378	N/A	0.56	19.77	N/A
108	NWB ch4 surface event NOAA	NOAA	39.34	-76.69	189.89	53	N/A	-27.09	62.22	N/A
109	NWF ch4 surface event NOAA	NOAA	40.03	-105.43	3067.68	880	N/A	1.87	20.13	N/A
110	OHP ch4 surface hourly LSCE	LSCE	43.92	5.75	637.65	54626	N/A	11.06	18.3	N/A
111	OPE ch4 surface hourly ICOS	ICOS	48.56	5.5	449.9	124659	N/A	8.19	26.8	N/A
112	ORC ch4 aircraft minute NOAA	NOAA	-46.21	-72.31	7297.29	6108	N/A	10.24	34.44	N/A
113	OXK ch4 surface hourly ICOS	ICOS	50.03	11.81	1113.65	47602	N/A	-15.43	24.19	N/A
114	PAL ch4 surface hourly FMI	FMI	67.97	24.12	567	131491	N/A	-5.59	13.57	N/A
115	PAL ch4 surface hourly ICOS	ICOS	67.97	24.12	577	33955	N/A	-7.4	14.35	N/A
116	PAO ch4 surface event NOAA	NOAA	18.23	-72.79	10	177	N/A	-0.84	11.49	N/A

117	PDI ch4 surface hourly EMPA	EMPA	21.57	103.52	1478	7037	N/A	-5.32	38.73	N/A
118	PDI ch4 surface hourly VNMHA	VNMHA	21.57	103.52	1478	40926	N/A	-18.77	41.09	N/A
119	PDM ch4 surface hourly LSCE	LSCE	42.94	0.14	2887	29118	N/A	-0.7	11.57	N/A
120	PRS ch4 surface hourly RSE	RSE	45.94	7.71	3490	77559	N/A	9.08	19.51	N/A
121	PUY ch4 surface hourly ICOS	ICOS	45.77	2.97	1475	42227	N/A	-10.75	16.22	N/A
122	PUY ch4 surface hourly LSCE	LSCE	45.77	2.97	1475	49795	N/A	-11.06	17.65	N/A
123	RGL ch4 surface hourly UNIVBRIS	UNIVBRIS	52	-2.54	275.89	73326	N/A	-11.93	33.36	N/A
124	RPB ch4 surface highfreq AGAGE	AGAGE	13.16	-59.43	42	10858	N/A	3.64	6.62	N/A
125	RUN ch4 surface hourly ICOS	ICOS	-21.08	55.38	2160	25300	N/A	-1.55	5.22	N/A
126	RYO ch4 surface hourly JMA	JMA	39.03	141.82	280	170510	N/A	-1.78	19.41	N/A
127	S2K ch4 aircraft event NOAA	NOAA	-23.92	29.37	4337.18	172	N/A	-8.9	37.78	N/A
128	SAC ch4 surface hourly ICOS	ICOS	48.72	2.14	221.79	91926	N/A	2.87	38.85	N/A
129	SCT ch4 surface hourly NOAA	NOAA	33.41	-81.83	235.25	145029	N/A	-6.07	55.35	N/A
130	SGP ch4 aircraft event NOAA	NOAA	36.8	-97.5	4459.11	7722	N/A	-4.07	19.7	N/A
131	SGP ch4 surface event NOAA	NOAA	36.61	-97.49	328.07	2461	N/A	-12.56	40.26	N/A
132	SMO ch4 surface highfreq AGAGE	AGAGE	-14.25	-170.56	77	11671	N/A	-2.24	5.74	N/A
133	SMR ch4 surface hourly ICOS	ICOS	61.85	24.29	250.56	118630	N/A	3.92	14.4	N/A
134	SOD ch4 surface hourly FMI	FMI	67.36	26.64	227	45822	N/A	-13.85	29.53	N/A
135	SSL ch4 surface hourly UBA	UBA	47.92	7.92	1217	8273	N/A	-0.56	22.27	N/A
136	SSL ch4 surface hourly UBAG	UBAG	47.9	7.92	1215.29	140689	N/A	2.25	22.15	N/A
137	STE ch4 surface hourly ICOS	ICOS	53.04	8.46	164.87	88652	N/A	-16.36	80.1	N/A
138	STR ch4 surface event NOAA	NOAA	37.76	-122.45	370	6800	N/A	4.42	7.97	N/A
139	SVB ch4 surface hourly ICOS	ICOS	64.26	19.77	325.08	105509	N/A	-0.97	12.54	N/A
140	SVV ch4 surface hourly NIES	NIES	51.33	82.13	534.49	11085	N/A	-182.41	113.56	N/A
141	TAC ch4 surface hourly UNIVBRIS	UNIVBRIS	52.52	1.14	178.43	68199	N/A	5.89	33.68	N/A
142	TAO ch4 surface hourly EC	EC	43.66	-79.4	100	16708	N/A	-23.17	53.92	N/A
143	THD ch4 surface highfreq AGAGE	AGAGE	41.05	-124.15	140	11287	N/A	2.5	17.64	N/A
144	TIK ch4 surface hourly FMI	FMI	71.6	128.89	29	75491	N/A	-4.28	25.95	N/A
145	TLL ch4 surface hourly DMC	DMC	-30.17	-70.8	2159	48055	N/A	-2.26	9.01	N/A
146	TLL ch4 surface hourly EMPA	EMPA	-30.17	-70.8	2225	7406	N/A	-2.66	5.34	N/A
147	TOH ch4 surface hourly ICOS	ICOS	51.81	10.53	886.58	125927	N/A	-4.67	21.41	N/A
148	TOM ch4 aircraft event NOAA	NOAA	11.22	-82.32	5281.65	1229	N/A	2.26	22.59	N/A
149	TPD ch4 surface hourly EC	EC	42.64	-80.56	266	67411	N/A	17.21	48.51	N/A

150	TPI ch4 surface event NOAA	NOAA	10.38	114.37	9	249	N/A	-2.16	16.83	N/A
151	TRN ch4 surface hourly ICOS	ICOS	47.96	2.11	214.48	143295	N/A	9.92	31.03	N/A
152	TRN ch4 surface hourly LSCE	LSCE	47.96	2.11	311	27395	N/A	11.91	31.41	N/A
153	TTA ch4 surface hourly UOB	UOB	56.56	-2.99	622	40878	N/A	-7.14	18.52	N/A
154	ULD ch4 surface hourly KMA	KMA	37.48	130.9	220.9	54305	N/A	-4.08	29.19	N/A
155	UTO ch4 surface hourly FMI	FMI	59.78	21.37	64	43561	N/A	4.42	14.72	N/A
156	UTO ch4 surface hourly ICOS	ICOS	59.78	21.37	65	28781	N/A	4.12	12.62	N/A
157	VGN ch4 surface hourly NIES	NIES	54.5	62.32	252	15037	N/A	-5.24	32.85	N/A
158	VKV ch4 surface hourly MGO	MGO	59.95	30.7	76	25870	N/A	-52.58	104.47	N/A
159	VRS ch4 surface event MPI-BGC	MPI-BGC	81.58	-16.64	24	94	N/A	2.29	9.09	N/A
160	WGC ch4 surface hourly NOAA	NOAA	38.26	-121.49	185.76	343102	N/A	-49.96	174.16	N/A
161	WKT ch4 surface event NOAA	NOAA	31.32	-97.32	260.26	4060	N/A	-13.62	38.12	N/A
162	WSA ch4 surface hourly EC	EC	43.93	-60.01	30	98715	N/A	-2.97	13.2	N/A
163	YAK ch4 surface hourly NIES	NIES	62.09	129.36	302.77	10654	N/A	-13.14	38.55	N/A
164	YON ch4 surface hourly JMA	JMA	24.47	123.01	50	168060	N/A	-2.65	22.84	N/A
165	ZEP ch4 surface hourly ICOS	ICOS	78.91	11.89	489	31923	N/A	4.38	9.4	N/A
166	ZEP ch4 surface hourly NILU	NILU	78.91	11.89	489	68159	N/A	4.52	24.1	N/A
167	ZGT ch4 surface hourly UBA	UBA	54.43	12.73	7.5	8360	N/A	-20.5	59.25	N/A
168	ZOT ch4 surface event MPI-BGC	MPI-BGC	60.75	89.38	111	764	N/A	-0.3	31.5	N/A
169	ZSF ch4 surface hourly UBA	UBA	47.42	10.98	2670	8287	N/A	-9.13	22.85	N/A
170	ZSF ch4 surface hourly UBAG	UBAG	47.42	10.98	2670	148212	N/A	-1.56	25.03	N/A

Table 5. Summary of statistics of observational Sites for $\delta^{13}C$-CH_4 used in CarbonTracker-CH_4

Assimilated										
	Site Code	**Laboratory**	**Latitude**	**Longitude**	**Elevation (MASL)**	**No. of Observation**	**Model-data mismatch**	**Mean bias**	**Standard deviation of bias**	**Chi-squared**
1	ALK ch4 aircraft event TU	TU	65.88	-152.16	2092.95	63	0.18	0.01	0.1	0.31
2	ALT ch4 surface event MPI-BGC	MPI-BGC	82.45	-62.51	185	220	0.28	0.07	0.14	0.31

3	ALT ch4 surface event NOAA	NOAA	82.45	-62.51	190	1809	0.1	0.03	0.11	2.12
4	AMY ch4 surface event NOAA	NOAA	36.54	126.33	87	335	0.08	0	0.15	4.43
5	ARH ch4 surface event NIWA	NIWA	-77.83	166.2	184	189	0.08	-0.02	0.05	0.43
6	ASC ch4 surface event NOAA	NOAA	-7.97	-14.4	90	2277	0.12	-0.02	0.1	1.38
7	AZR ch4 surface event NOAA	NOAA	38.76	-27.33	24	729	0.09	0.01	0.12	1.88
8	BAL ch4 surface event NOAA	NOAA	55.35	17.22	28	394	0.15	0.07	0.14	3.74
9	BHD ch4 surface event NIWA	NIWA	-41.41	174.87	85	311	0.08	-0.07	0.06	1.25
10	BHD ch4 surface event NOAA	NOAA	-41.41	174.87	92.46	238	0.1	-0.06	0.09	2.52
11	BIK ch4 surface event MPI-BGC	MPI-BGC	53.2	22.75	183	139	0.31	0	0.19	0.4
12	BMW ch4 surface event NOAA	NOAA	32.26	-64.88	51.3	2	0.15	-0.07	0.03	0.22
13	BRW ch4 surface event NOAA	NOAA	71.32	-156.61	21.66	2544	0.11	0.08	0.14	4.93
14	BSC ch4 surface event NOAA	NOAA	44.18	28.66	5	20	0.09	-0.07	0.16	3.28
15	CBA ch4 surface event NOAA	NOAA	55.21	-162.72	57.04	1591	0.1	0.12	0.12	5.52
16	CGO ch4 surface event NOAA	NOAA	-40.68	144.68	164	1050	0.09	-0.04	0.1	1.79
17	CHR ch4 surface event NOAA	NOAA	1.7	-157.15	5	12	0.08	0.04	0.14	3.13
18	CIB ch4 surface event NOAA	NOAA	41.81	-4.93	850	2	0.05	-0.19	0.04	16.53
19	CON ch4 aircraft event TU	TU	9.02	134.97	11131.5	414	0.18	0.04	0.11	0.48
20	CVO ch4 surface event MPI-BGC	MPI-BGC	16.86	-24.87	10	413	0.27	0.01	0.13	0.22
21	DRP ch4 surface event NOAA	NOAA	-57.25	-64.26	10	2	0.06	-0.06	0.05	1.25
22	EIC ch4 surface event NOAA	NOAA	-27.16	-109.43	69	150	0.08	-0.07	0.07	2.11
23	GMI ch4 surface event NOAA	NOAA	13.39	144.66	5	336	0.11	0	0.11	1.38
24	HSU ch4 surface event NOAA	NOAA	41.05	-124.58	7.6	2	0.08	0.26	0.14	19.83
25	INX ch4 surface event NOAA	NOAA	39.58	-86.42	376.73	30	0.09	-0.11	0.13	1.51
26	JFJ ch4 surface event MPI-BGC	MPI-BGC	46.55	7.99	3570	158	0.3	0.03	0.14	0.25
27	KCO ch4 surface event NOAA	NOAA	4.97	73.47	6	4	0.08	0.01	0.07	0.49
28	KJO ch4 surface event MPI-BGC	MPI-BGC	70.85	29.24	5	169	0.26	0.16	0.14	0.69

29	KUM ch4 surface event NOAA	NOAA	19.54	-154.84	7.44	1431	0.12	-0.01	0.09	1.37
30	LLB ch4 surface event NOAA	NOAA	54.95	-112.45	572.1	253	0.12	-0.05	0.28	8.27
31	LLN ch4 surface event NOAA	NOAA	23.47	120.87	2867	2	0.05	-0.36	0.11	55.27
32	MEX ch4 surface event NOAA	NOAA	18.98	-97.31	4469	655	0.14	-0.01	0.11	1.96
33	MHD ch4 surface event NOAA	NOAA	53.32	-9.9	26.14	1065	0.12	0	0.11	1.72
34	MID ch4 surface event NOAA	NOAA	28.21	-177.38	13.78	405	0.09	0	0.1	1.95
35	MLO ch4 surface event NOAA	NOAA	19.53	-155.57	3419.3	2739	0.11	-0.01	0.1	1.33
36	NMB ch4 surface event MPI-BGC	MPI-BGC	-23.58	15.03	456	244	0.26	-0.06	0.55	1.86
37	NWR ch4 surface event NOAA	NOAA	40.05	-105.58	3526	1396	0.1	-0.03	0.1	1.84
38	NYA ch4 surface event TU	TU	78.92	11.93	43	900	0.16	0.09	0.11	0.81
39	OXK ch4 surface event MPI-BGC	MPI-BGC	50.03	11.81	1022	82	0.31	0.04	0.19	0.47
40	PFA ch4 aircraft event NOAA	NOAA	64.85	-148.7	2981.09	1339	0.11	0.07	0.26	9.73
41	POC ch4 surface event NIWA	NIWA	0.71	133.13	24.17	270	0.16	0.01	0.06	0.15
42	PSA ch4 surface event NOAA	NOAA	-64.77	-64.05	15	9	0.08	0.17	0.16	8.23
43	SDZ ch4 surface event NOAA	NOAA	40.65	117.12	298	6	0.1	-0.02	0.1	1.13
44	SGP ch4 aircraft event NOAA	NOAA	36.61	-97.49	2407.51	12	0.07	0.03	0.11	2.74
45	SIS ch4 surface event MPI-BGC	MPI-BGC	60.09	-1.25	30	447	0.29	0.05	0.17	0.38
46	SMO ch4 surface event NOAA	NOAA	-14.25	-170.57	53.35	2516	0.1	0	0.09	1.28
47	SPO ch4 surface event NOAA	NOAA	-89.98	-24.8	2817.21	2125	0.1	-0.03	0.1	1.55
48	SUM ch4 surface event NOAA	NOAA	72.6	-38.42	3214.54	762	0.1	0.03	0.11	2.41
49	TAC ch4 surface event NOAA	NOAA	52.52	1.14	236	73	0.06	0.01	0.12	4.19
50	TAP ch4 surface event NOAA	NOAA	36.73	126.13	21	955	0.1	-0.01	0.16	4.12
51	WGC ch4 surface event NOAA	NOAA	38.26	-121.49	91.1	65	0.12	-0.27	0.56	35.3
52	WLG ch4 surface event NOAA	NOAA	36.29	100.9	3815	1038	0.1	-0.04	0.11	2.5
53	WPC ch4 surface event NOAA	NOAA	1.42	150.92	10	222	0.1	0.02	0.13	1.71

54	ZEP ch4 surface event NOAA	NOAA	78.91	11.89	479	935	0.1	0.04	0.13	2.65
Unassimilated										
	Site Code	**Laboratory**	**Latitude**	**Longitude**	**Elevation (MASL)**	**No. of Observation**	**Model-data mismatch**	**Mean bias**	**Standard deviation of bias**	**Chi-squared**
1	ACG ch4 aircraft event NOAA	NOAA	68.38	-152.32	2735.44	649	N/A	0.09	0.25	N/A
2	ACT ch4 aircraft event NOAA	NOAA	37.68	-87.69	2119.47	1267	N/A	-0.03	0.21	N/A
3	CRV ch4 aircraft event NOAA	NOAA	65.59	-150.75	1402.76	1722	N/A	0.31	0.42	N/A
4	CRV ch4 surface event NOAA	NOAA	64.99	-147.6	643.13	1056	N/A	0.11	0.24	N/A
5	CVO ch4 surface event MPI-BGC	MPI-BGC	16.86	-24.87	10	413	N/A	-0.1	0	N/A
6	GVN ch4 surface event MPI-BGC	MPI-BGC	-70.67	-8.27	40	114	N/A	-0.37	0.43	N/A
7	HIP ch4 aircraft event NOAA	NOAA	18.16	-94.78	4776.61	463	N/A	0.11	0.33	N/A
8	INX ch4 aircraft event NOAA	NOAA	39.86	-86.06	801.16	149	N/A	0.08	0.28	N/A
9	INX ch4 surface event NOAA	NOAA	39.77	-86.1	267.92	30	N/A	-0.26	0.49	N/A
10	JFJ ch4 surface event MPI-BGC	MPI-BGC	46.55	7.99	3570	158	N/A	0.08	0	N/A
11	MRC ch4 aircraft event NOAA	NOAA	41.73	-76.26	1285.3	65	N/A	-0.1	0.15	N/A
12	MRC ch4 surface event NOAA	NOAA	41.53	-76.27	623.56	704	N/A	-0.13	0.21	N/A
13	NGM ch4 surface event TU	TU	-0.94	148.54	20	466	N/A	0	0.13	N/A
14	NSA ch4 aircraft event NOAA	NOAA	70.02	-151.02	1083.82	112	N/A	0.06	0.43	N/A
15	TOM ch4 aircraft event NOAA	NOAA	11.52	-79.49	5228.24	1085	N/A	-0.02	0.19	N/A
16	VRS ch4 surface event MPI-BGC	MPI-BGC	81.58	-16.64	24	23	N/A	0.13	0.26	N/A
17	ZOT ch4 surface event MPI-BGC	MPI-BGC	60.75	89.38	111	527	N/A	0.15	0.34	N/A

C. Atmospheric inversion setup

1. The TM5 Atmospheric Transport Model

The global chemistry Transport Model, version 5 (TM5) is developed and maintained jointly by the Institute for Marine and Atmospheric Research Utrecht (IMAU, the Netherlands), the Joint Research Centre (JRC, Italy), the Royal Netherlands Meteorological Institute (KNMI, the Netherlands), and the National Oceanic & Atmospheric Administration (NOAA) Global Monitoring Laboratory (GML, USA) (Krol et al. 2005; Bruhwiler et al. 2014; Peters et al. 2007). The model simulates atmospheric transport using input from the European Center for Medium range Weather Forecast (ECMWF) model. TM5 has detailed treatments of advection, convection (deep and shallow), and vertical diffusion in the planetary boundary layer and free troposphere.

The winds which drive TM5 come from the ECMWF operational forecast model. This "parent" model currently runs with ~25 km horizontal resolution and 60 layers in the vertical before 2006 (and 91 layers in the vertical from 2006 onwards). Since the ERA-interim product is not available after September 2019, we switched out meteorological inputs from ERA-interim to ERA-5, which covers the Earth on a 30 km grid and resolves the atmosphere using 137 levels from the surface up to a height of 80km (Hersbach et al. 2020).

For use in TM5, the ECMWF meteorological data are preprocessed into mass fluxes at coarser horizontal and vertical resolution. In this release of CarbonTracker-CH_4, TM5 is run at a global 3°x 2° spatial resolution and 30-minute temporal resolution. The vertical resolution of TM5 in CarbonTracker-CH_4 is 25 hybrid sigma-pressure levels. The approximate heights of the mid-levels (in meters, with a surface pressure of 1012 hPa) are summarized in Table 6.

Table 6. Approximate heights of the vertical model layers.

Level	Height (m)	Level	Height (m)
1	34.5	14	9076.6
2	111.9	15	10533.3
3	256.9	16	12108.3
4	490.4	17	13874.2
5	826.4	18	15860.1
6	1274.1	19	18093.2
7	1839	20	20590
8	2524	21	24247.3

9	3329.9	22	29859.6
10	4255.6	23	35695
11	5298.5	24	42551.5
12	6453.8	25	80000
13	7715.4		

2. 4DVAR inversion setup

2.1. Inversion framework

We use the TM5-4DVAR inversion framework (Meirink et al. 2008), which has been used to estimate surface fluxes of CO, CO_2, and CH_4 (Hooghiemstra and van Ees 2011; Bergamaschi et al. 2013; Krol et al. 2013; Basu et al. 2014) in single-tracer inversions, as well as source-specific CO_2 fluxes in multi-tracer inversions (Ma et al. 2021; Basu et al. 2020; Basu et al. 2022).

Two tracers are simulated in our inversion: total CH_4 or *C* and the artificial tracer *Cxδ'*, where $\delta' = (^{13}CH_4/CH_4)/r_{std}-1$. More details can be found in (Basu et al. 2022). TM5-4DVAR minimizes a cost function *J* in equation below, as a function of surface fluxes *x* by balancing fits to atmospheric observations *y* with deviations from the prior fluxes x_0,

$$J(x) = 1/2\ (Hx-y)^T R^{-1}(Hx-y) + 1/2(x-x_0)^T B^{-1}(x-x_0)$$

where *H* is the transport, chemistry, and observation operator connecting surface fluxes with atmospheric measurements, and *R* and *B* are the error covariances of *Hx−y* and prior fluxes, respectively, and R was set based on the model-data mismatch setup (Tables 3-4). From the inversion, we optimize monthly surface fluxes (*x*, posterior flux) for microbial, fossil, and pyrogenic sources at 3°x 2° spatial resolution.

2.2. Prior error covariance

For each source type (pyrogenic, fossil, and microbial), the diagonal elements of *B* per time step and lateral grid cell are proportional (f in Table 7) to the prior flux (x_0), or $f \times x_0$. Off-diagonal elements of *B* are constructed assuming an exponential decay of the prior error correlation in space and time with source-specific scales *λ* and *τ*, respectively. By following Basu et al. (2022), we also followed the source-specific scales to be the same as Table 7.

Table 7. Parameters for constructing the prior flux error covariance.

	Diagonal uncertainty (f, %)	Off-diagonal spatial (λ, km)	Off-diagonal temporal (τ, months)
Microbial	120	500	2
Fossil	150	700	6
Pyrogenic	100	300	1

2.3. Simulation setup

The cost function J is minimized over 65-100 iterations by an M1QN3 minimizer, which utilizes a limited memory quasi-Newton technique (the L-BFGS method of J. Nocedal) with a dynamically updated scalar or diagonal preconditioner. Due to the long computation time for inversion, we split our simulation periods into 8 inversions that were run in parallel. Eight 5-year inversions were run simultaneously with 2 years of overlap (first and last years) between inversions, starting in 1997, 2000, 2003, 2006, 2009, 2012, 2015, and 2017. After all eight inversions finished, the fluxes from the middle 3-year period of each inversion were considered for analysis. For simulating prior and posterior mole fractions, fluxes from the non-overlapping periods were stitched together and a single forward run was done with those long-term posterior fluxes.

2.4. Uncertainty estimation

We estimated the uncertainty of our simulation using 100 ensemble members with different random uncertainties in prior flux and observations. The random uncertainties are associated with components of the inversion system whose errors are assumed to be zero on average. We construct the ensembles with prior fluxes and observations perturbed according to the covariances specified by B and R, respectively. With 100 ensemble members, our estimate is expected to be within 10 % of the exact analytical solution. More information can be found in (Basu et al. 2022).

D. Outputs

Spatial flux maps and bar charts of optimized emissions can be found at https://gml.noaa.gov/ccgg/carbontracker-ch4/fluxes.html. These pages give access to maps and bar charts illustrating the estimated microbial, fossil, and pyrogenic CH_4 emission fluxes. On the flux maps page, users may select the entire time period, a single month, or a year at different regions to see prior and posterior CH_4 fluxes of microbial, fossil, and pyrogenic sources. Flux bar charts pages show long-term prior and posterior CH_4 fluxes of microbial, fossil, and pyrogenic sources at monthly and yearly timescale.

Second, evaluation and observation tabs are available to compare the simulated atmospheric CH_4 and $\delta^{13}C\text{-}CH_4$ with observations using various metrics: https://gml.noaa.gov/ccgg/carbontracker-ch4/network_map3.html and https://gml.noaa.gov/ccgg/carbontracker-ch4/evaluation.html. Specifically, we provide interactive plots of time series of atmospheric CH_4 and $\delta^{13}C\text{-}CH_4$, prior, post-assimilation (posterior), and observed, at each observation site and aircraft profile. We provide three diagnostics to evaluate this version of inversion system: (1) Comparison of prior, posterior, and observed atmospheric CH_4 and $\delta^{13}C\text{-}CH_4$ from all assimilated and un-assimilated sites, (2) Comparison of posterior and observed CH_4 and $\delta^{13}C\text{-}CH_4$ for independent Aircraft Profiles, and (3) Large-scale averages and growth rates of prior, posterior, and observed atmospheric CH_4 and $\delta^{13}C\text{-}CH_4$.

Third, three-dimensional atmospheric methane concentrations simulated with optimized emissions by CarbonTracker-CH_4 are visualized as sphere and 3-D volume plots at monthly timescale: https://gml.noaa.gov/ccgg/carbontracker-ch4/visualization.html.

Lastly, users can download the optimized (posterior) surface emissions from microbial, fossil, and pyrogenic sources (3x2°, monthly) and optimized 4-dimensional atmospheric CH_4 mole fractions (3x2° horizontal grids and 25 vertical layers, 3-hourly) globally from this page: https://gml.noaa.gov/ccgg/carbontracker-ch4/download.html.

E. References

Abbott, D. W., Aasen, I. M., Beauchemin, K. A., Grondahl, F., Gruninger, R., Hayes, M., Huws, S., Kenny, D. A., Krizsan, S. J., Kirwan, S. F., Lind, V., Meyer, U., Ramin, M., Theodoridou, K., von Soosten, D., Walsh, P. J., Waters, S., & Xing, X. (2020). Seaweed and Seaweed Bioactives for Mitigation of Enteric Methane: Challenges and Opportunities. *Animals : An Open Access Journal from MDPI*, *10*(12). https://doi.org/10.3390/ani10122432

Andrews, A. E., Kofler, J. D., Trudeau, M. E., Williams, J. C., Neff, D. H., Masarie, K. A., Chao, D. Y., Kitzis, D. R., Novelli, P. C., Zhao, C. L., & Others. (2014). CO_2, CO, and CH_4 measurements from tall towers in the NOAA Earth System Research Laboratory's Global Greenhouse Gas Reference Network: Instrumentation, uncertainty analysis, and recommendations for future high-accuracy greenhouse gas monitoring efforts. *Atmospheric Measurement Techniques*, *7*(2), 647.

Basu, S., Krol, M., Butz, A., Clerbaux, C., Sawa, Y., Machida, T., Matsueda, H., Frankenberg, C., Hasekamp, O. P., & Aben, I. (2014). The seasonal variation of the CO2 flux over Tropical Asia estimated from GOSAT, CONTRAIL, and IASI. *Geophysical Research Letters*, *41*(5), 1809–1815.

Basu, S., Lan, X., Dlugokencky, E., Michel, S., Schwietzke, S., Miller, J. B., Bruhwiler, L., Oh, Y., Tans, P. P., Apadula, F., & Others. (2022). Estimating emissions of methane consistent with atmospheric measurements of methane and $\delta^{13}C$ of methane. *Atmospheric Chemistry and Physics*, *22*(23), 15351–15377.

Bergamaschi, P., Houweling, S., Segers, A., Krol, M., Frankenberg, C., Scheepmaker, R. A., Dlugokencky, E., Wofsy, S. C., Kort, E. A., Sweeney, C., Schuck, T., Brenninkmeijer, C., Chen, H., Beck, V., & Gerbig, C. (2013). Atmospheric CH_4 in the first decade of the 21st century: Inverse modeling analysis using SCIAMACHY satellite retrievals and NOAA surface measurements. *Journal of Geophysical Research, D: Atmospheres*, *118*(13), 7350–7369.

Bergamaschi, P., Krol, M., Dentener, F., Vermeulen, A., Meinhardt, F., Graul, R., Ramonet, M., Peters, W., Dlugokencky, E. J., Bergamaschi, P., Krol, M., Dentener, F., Vermeulen, A., & Meinhardt, F. (2005). *Inverse modelling of national and European CH_4 emissions using the atmospheric zoom model TM5. Atmospheric Chemistry and Physics, 5(9), 2431-2460.*

Bruhwiler, L., Dlugokencky, E., Masarie, K., Ishizawa, M., Andrews, A., Miller, J., Sweeney, C., Tans, P., & Worthy, D. (2014). CarbonTracker-CH_4: An assimilation system for estimating emissions of atmospheric methane. *Atmospheric Chemistry and Physics*, *14*(16), 8269–8293.

Cantrell, C. A., Shetter, R. E., McDaniel, A. H., Calvert, J. G., Davidson, J. A., Lowe, D. C., Tyler, S. C., Cicerone, R. J., & Greenberg, J. P. (1990). Carbon kinetic isotope effect in the oxidation of methane by the hydroxyl radical. *Journal of Geophysical Research, D: Atmospheres*, *95*(D13), 22455–22462.

Chang, J., Peng, S., Ciais, P., Saunois, M., Dangal, S. R. S., Herrero, M., Havlík, P., Tian, H., & Bousquet, P. (2019). Revisiting enteric methane emissions from domestic ruminants and their $\delta^{13}C$ CH_4 source signature. *Nature Communications*, *10*(1), 1–14.

Crippa, M., Guizzardi, D., Muntean, M., Schaaf, E., Solazzo, E., Monforti-Ferrario, F.,

Olivier, J. G. J., & Vignati, E. (2020). Fossil CO_2 emissions of all world countries. *Luxembourg: European Commission*, 1–244.
Etiope, G., Ciotoli, G., Schwietzke, S., & Schoell, M. (2019). Gridded maps of geological methane emissions and their isotopic signature. *Earth System Science Data*, *11*(1), 1–22.
Ganesan, A. L., Stell, A. C., Gedney, N., Comyn-Platt, E., Hayman, G., Rigby, M., Poulter, B., & Hornibrook, E. R. C. (2018). Spatially Resolved Isotopic Source Signatures of Wetland Methane Emissions. *Geophysical Research Letters*, *45*(8), 3737–3745.
Gromov, S., Brenninkmeijer, C. A. M., & Jöckel, P. (2018). A very limited role of tropospheric chlorine as a sink of the greenhouse gas methane. *Atmospheric Chemistry and Physics*, *18*(13), 9831–9843.
Hersbach, H., Bell, B., Berrisford, P., Hirahara, S., Horányi, A., Muñoz-Sabater, J., Nicolas, J., Peubey, C., Radu, R., Schepers, D., Simmons, A., Soci, C., Abdalla, S., Abellan, X., Balsamo, G., Bechtold, P., Biavati, G., Bidlot, J., Bonavita, M., … Jean-Noël Thépaut. (2020). The ERA5 global reanalysis. *Quarterly Journal of the Royal Meteorological Society*, *146*(730), 1999–2049.
Hooghiemstra, R., & van Ees, H. (2011). Uniformity as response to soft law: Evidence from compliance and non-compliance with the Dutch corporate governance code. *Regulation & Governance*, *5*(4), 480–498.
Hossaini, R., Chipperfield, M. P., Saiz‐Lopez, A., Fernandez, R., Monks, S., Feng, W., Brauer, P., & Von Glasow, R. (2016). A global model of tropospheric chlorine chemistry: Organic versus inorganic sources and impact on methane oxidation. *Journal of Geophysical Research, D: Atmospheres*, *121*(23), 14–271.
Janssens-Maenhout, G., Crippa, M., Guizzardi, D., Muntean, M., Schaaf, E., Dentener, F., Bergamaschi, P., Pagliari, V., Olivier, J. G. J., Peters, J. A., & Others. (2019). EDGAR v4. 3.2 Global Atlas of the three major greenhouse gas emissions for the period 1970--2012. *Earth System Science Data*, *11*(3), 959–1002.
Jöckel, P., Tost, H., Pozzer, A., Brühl, C., Buchholz, J., Ganzeveld, L., Hoor, P., Kerkweg, A., Lawrence, M. G., Sander, R., Steil, B., Stiller, G., Tanarhte, M., Taraborrelli, D., van Aardenne, J., & Lelieveld, J. (2006). The atmospheric chemistry general circulation model ECHAM5/MESSy1: consistent simulation of ozone from the surface to the mesosphere. *Atmospheric Chemistry and Physics*, *6*(12), 5067–5104.
Judd, A. G. (2004). Natural seabed gas seeps as sources of atmospheric methane. *Environmental Geology*, *46*(8), 988–996.
King S. L. Quay P. D. Lansdown J., M. (1989). The 13C/12C Kinetic Isotope Effect for Soil Oxidation of Methane increase. *Journal of Geophysical Research*, *94*, 273–277.
Krol, M., Houweling, S., Bregman, B., Broek, M. v., Segers, A., van Velthoven, P., Peters, W., Dentener, F., & Bergamaschi, P. (2005). The two-way nested global chemistry-transport zoom model TM5: algorithm and applications. *Atmospheric Chemistry and Physics*, *5*(2), 417–432.
Krol, M., Peters, W., Hooghiemstra, P., George, M., Clerbaux, C., Hurtmans, D., Mcinerney, D., Sedano, F., Bergamaschi, P., El Hajj, M., & Others. (2013). How much CO was emitted by the 2010 fires around Moscow? *Atmospheric Chemistry*

and Physics, *13*(9), 4737–4747.
Krol, M., van Leeuwen, P. J., & Lelieveld, J. (1998). Global OH trend inferred from methylchloroform measurements. *Journal of Geophysical Research*, *103*(D9), 10697–10711.
Lan, X., Basu, S., Schwietzke, S., Bruhwiler, L. P., Dlugokencky, E. J., Michel, S. E., Sherwood, O. A., Tans, P. P., Thoning, K. W., Etiope, G., Zhuang, Q., Liu, L., Oh, Y., Miller, J. B., Petron, G., Vaughn, B. H., Andrews, A. E., & Crippa, M. (2021). Improved constraints on global methane emissions and sinks using $\delta^{13}C\text{-}CH_4$. *Global Biogeochemical Cycles*.
Lee, J., Oh, Y., Lee, S. T., Seo, Y. O., Yun, J., Yang, Y., Kim, J., Zhuang, Q., & Kang, H. (2023). Soil organic carbon is a key determinant of CH_4 sink in global forest soils. *Nature Communications*, *14*(1), 3110.
Le Mer, J., & Roger, P. (2001). Production, oxidation, emission and consumption of methane by soils: a review. *European Journal of Soil Biology*, *37*(1), 25–50.
Liu, L., Zhuang, Q., Oh, Y., Shurpali, N. J., Kim, S., & Poulter, B. (2020). Uncertainty Quantification of Global Net Methane Emissions from Terrestrial Ecosystems Using a Mechanistically-based Biogeochemistry Model. *Journal of Geophysical Research: Biogeosciences*, *125(6)*, e2019JG005428.
Matthews E. and Fung, I. (1987). Methane emission from natural wetlands: Global distribution, area, and environmental characteristics of sources. *Global Biogeochemical Cycles*, *1*(1), 61–86.
McNicol, G., Fluet-Chouinard, E., Ouyang, Z., Knox, S., Zhang, Z., Aalto, T., Bansal, S., Chang, K.-Y., Chen, M., Delwiche, K., Feron, S., Goeckede, M., Liu, J., Malhotra, A., Melton, J. R., Riley, W., Vargas, R., Yuan, K., Ying, Q., … Jackson, R. B. (2023). Upscaling wetland methane emissions from the FLUXNET-CH_4 eddy covariance network (UpCH$_4$ v1.0): Model development, network assessment, and budget comparison. *AGU Advances*, *4*(5). https://doi.org/10.1029/2023av000956
Meirink, J. F., Bergamaschi, P., & Krol, M. C. (2008). Four-dimensional variational data assimilation for inverse modelling of atmospheric methane emissions: method and comparison with synthesis inversion. *Atmospheric Chemistry and Physics*, *8*(21), 6341–6353.
Miller, J. B., Mack, K. A., Dissly, R., White, J. W. C., Dlugokencky, E. J., & Tans, P. P. (2002). Development of analytical methods and measurements of 13C/12C in atmospheric CH4 from the NOAA Climate Monitoring and Diagnostics Laboratory Global Air Sampling Network. *Journal of Geophysical Research, D: Atmospheres*, *107*(13).
Montzka, S. A., Krol, M., Dlugokencky, E., Hall, B., Jöckel, P., & Lelieveld, J. (2011). Small interannual variability of global atmospheric hydroxyl. *Science*, *331*(6013), 67–69.
Oh, Y., Zhuang, Q., Liu, L., Welp, L. R., Lau, M. C. Y., Onstott, T. C., Medvigy, D., Bruhwiler, L., Dlugokencky, E. J., Hugelius, G., D'Imperio, L., & Elberling, B. (2020). Reduced net methane emissions due to microbial methane oxidation in a warmer Arctic. *Nature Climate Change*, *10*(4), 317–321.
Patra, P. K., Krol, M. C., Montzka, S. A., Arnold, T., Atlas, E. L., Lintner, B. R., Stephens, B. B., Xiang, B., Elkins, J. W., Fraser, P. J., Ghosh, A., Hintsa, E. J., Hurst, D. F., Ishijima, K., Krummel, P. B., Miller, B. R., Miyazaki, K., Moore, F. L., Mühle, J., …

Young, D. (2014). Observational evidence for interhemispheric hydroxyl-radical parity. *Nature*, *513*(7517), 219–223.
Peters, W., Jacobson, A. R., Sweeney, C., Andrews, A. E., Conway, T. J., Masarie, K., Miller, J. B., Bruhwiler, L. M. P., Pétron, G., Hirsch, A. I., Worthy, D. E. J., van der Werf, G. R., Randerson, J. T., Wennberg, P. O., Krol, M. C., & Tans, P. P. (2007). An atmospheric perspective on North American carbon dioxide exchange: CarbonTracker. *Proceedings of the National Academy of Sciences of the United States of America*, *104*(48), 18925–18930.
Randerson, J. T., Chen, Y., Van Der Werf, G. R., Rogers, B. M., & Morton, D. C. (2012). Global burned area and biomass burning emissions from small fires. *Journal of Geophysical Research: Biogeosciences*, *117*(G4).
Randerson, J. T., Werf, G. R. van der, Giglio, L., Collatz, G. J., & Kasibhatla., P. S. (2018). *Global Fire Emissions Database, Version 4.1 (GFEDv4)*. ORNL DAAC, Oak Ridge, Tennessee, USA.
Ren, T., & Patel, M. K. (2009). Basic petrochemicals from natural gas, coal and biomass: Energy use and CO_2 emissions. *Resources, Conservation and Recycling*, *53*(9), 513–528.
Rosentreter, J. A., Borges, A. V., Deemer, B. R., Holgerson, M. A., Liu, S., Song, C., Melack, J., Raymond, P. A., Duarte, C. M., & Allen, G. H. (2021). Half of global methane emissions come from highly variable aquatic ecosystem sources. *Nature Geoscience*, *14*(4), 225–230.
Saitoh, N., Kimoto, S., Sugimura, R., Imasu, R., Kawakami, S., Shiomi, K., Kuze, A., Machida, T., Sawa, Y., & Matsueda, H. (2015). Validation of GOSAT/TANSO-FTS TIR UTLS CO2 data (Version 1.0) using CONTRAIL measurements. *Atmos. Meas. Tech. Discuss*, *8*, 12993–13037.
Saueressig, Gerd, P. Bergamaschi, J. N. Crowley, H. Fischer, and G. W. Harris. "Carbon kinetic isotope effect in the reaction of CH_4 with Cl atoms." *Geophysical Research Letters* 22, no. 10 (1995): 1225-1228.
Saueressig, G., Crowley, J. N., Bergamaschi, P., Brühl, C., Brenninkmeijer, C. A. M., & Fischer, H. (2001). Carbon 13 and D kinetic isotope effects in the reactions of CH_4 with O (1 D) and OH: new laboratory measurements and their implications for the isotopic composition of stratospheric methane. *Journal of Geophysical Research, D: Atmospheres*, *106*(D19), 23127–23138.
Saunois, M., Stavert, A. R., Poulter, B., Bousquet, P., Canadell, J. G., Jackson, R. B., Raymond, P. A., Dlugokencky, E. J., & Houweling, S. (2020). *The Global Methane Budget 2000 – 2017*. 1561–1623.
Schuur, E. A. G., Abbott, B. W., Commane, R., Ernakovich, J., Euskirchen, E., Hugelius, G., Grosse, G., Jones, M., Koven, C., Leshyk, V., Lawrence, D., Loranty, M. M., Mauritz, M., Olefeldt, D., Natali, S., Rodenhizer, H., Salmon, V., Schädel, C., Strauss, J., … Turetsky, M. (2022). Permafrost and Climate Change: Carbon Cycle Feedbacks From the Warming Arctic. *Annual Review of Environment and Resources*, *47*(1), 343–371.
Sherwood, O. A., Schwietzke, S., Arling, V. A., & Etiope, G. (2017). Global inventory of gas geochemistry data from fossil fuel, microbial and burning sources, version 2017. *Earth System Science Data*, *9*(2), 639–656.
Sherwood, O. A., Schwietzke, S., & Lan, X. (2021). Global $\delta^{13}C\text{-}CH_4$ source signature

inventory 2020. NOAA *Monitoring Laboratory Data Repository*.
Spivakovsky, C. M., Logan, J. A., Montzka, S. A., Balkanski, Y. J., Foreman-Fowler, M., Jones, D. B. A., Horowitz, L. W., Fusco, A. C., Brenninkmeijer, C. A. M., & Prather, M. J. (2000). Three-dimensional climatological distribution of tropospheric OH: Update and evaluation. *Journal of Geophysical Research, D: Atmospheres*, *105*(D7), 8931–8980.
Still, C. J., Berry, J. A., Collatz, G. J., & DeFries, R. S. (2003). Global distribution of C3 and C4 vegetation: Carbon cycle implications. *Global Biogeochemical Cycles*, *17*(1), 6–1 – 6–14.
Strode, S. A., Wang, J. S., Manyin, M., Duncan, B., Hossaini, R., Keller, C. A., Michel, S. E., & White, J. W. C. (2020). Strong sensitivity of the isotopic composition of methane to the plausible range of tropospheric chlorine. *Atmospheric Chemistry and Physics*, *20*(14), 8405–8419.
Sweeney, C., Karion, A., Wolter, S., Newberger, T., Guenther, D., Higgs, J. A., Andrews, A. E., Lang, P. M., Neff, D., Dlugokencky, E., Miller, J. B., Montzka, S. A., Miller, B. R., Masarie, K. A., Biraud, S. C., Novelli, P. C., Crotwell, M., Crotwell, A. M., Thoning, K., & Tans, P. P. (2015). Seasonal climatology of CO2 across North America from aircraft measurements in the NOAA/ESRL Global Greenhouse Gas Reference Network. *Journal of Geophysical Research*, *120*(10), 5155–5190.
Themelis, N. J., & Bourtsalas, A. C. (2021). Methane generation and capture of US landfills. *J. Environ. Sci. Eng. A*, *10*, 199–206.
Thompson, C. R., Wofsy, S. C., Prather, M. J., Newman, P. A., Hanisco, T. F., Ryerson, T. B., Fahey, D. W., Apel, E. C., Brock, C. A., Brune, W. H., & Others. (2022). The NASA Atmospheric Tomography (ATom) mission: Imaging the chemistry of the global atmosphere. *Bulletin of the American Meteorological Society*, *103*(3), E761–E790.
Umezawa, T., Machida, T., Ishijima, K., Matsueda, H., Sawa, Y., Patra, P. K., Aoki, S., & Nakazawa, T. (2012). Carbon and hydrogen isotopic ratios of atmospheric methane in the upper troposphere over the Western Pacific. *Atmospheric Chemistry and Physics*, *12*(17), 8095–8113.
Van Der Werf, G. R., Randerson, J. T., Giglio, L., Van Leeuwen, T. T., Chen, Y., Rogers, B. M., Mu, M., Van Marle, M. J. E., Morton, D. C., Collatz, G. J., & Others. (2017). Global fire emissions estimates during 1997--2016. *Earth System Science Data*, *9*(2), 697–720.
Wofsy, S. C. (2011). HIAPER Pole-to-Pole Observations (HIPPO): fine-grained, global-scale measurements of climatically important atmospheric gases and aerosols. *Philosophical Transactions of the Royal Society A: Mathematical, Physical and Engineering Sciences*, *369*(1943), 2073–2086.
Zhang, Z., Poulter, B., Feldman, A. F., Ying, Q., Ciais, P., Peng, S., & Li, X. (2023). Recent intensification of wetland methane feedback. *Nature Climate Change*, *13*(5), 430–433.
Zhang, Z., Zimmermann, N. E., Stenke, A., Li, X., Hodson, E. L., Zhu, G., Huang, C., & Poulter, B. (2017). Emerging role of wetland methane emissions in driving 21st century climate change. *Proceedings of the National Academy of Sciences of the United States of America*, *114*(36), 9647–9652.
Zhou, L., Warner, J., Nalli, N. R., Wei, Z., Oh, Y., Bruhwiler, L., Liu, X., Divakarla, M.,

Pryor, K., Kalluri, S., & Goldberg, M. D. (2023). Spatiotemporal Variability of Global Atmospheric Methane Observed from Two Decades of Satellite Hyperspectral Infrared Sounders. *Remote Sensing*, *15*(12), 2992.

Zhuang, Q., Guo, M., Melack, J. M., Lan, X., Tan, Z., Oh, Y., & Leung, L. R. (2023). Current and future global lake methane emissions: A process‐based modeling analysis. *Journal of Geophysical Research. Biogeosciences*, *128*(3). https://doi.org/10.1029/2022jg007137

Zhuang, Q., Melillo, J. M., Kicklighter, D. W., Prinn, R. G., McGuire, A. D., Steudler, P. A., Felzer, B. S., & Hu, S. (2004). Methane fluxes between terrestrial ecosystems and the atmosphere at northern high latitudes during the past century: A retrospective analysis with a process-based biogeochemistry model. *Global Biogeochemical Cycles*, *18*(3). https://doi.org/10.1029/2004GB002239

Zhuang, Q., Xu, K., Tang, J., Saikawa, E., Lu, Y., Melillo, J. M., Prinn, R. G., & McGuire, A. D. (2013). Response of global soil consumption of atmospheric methane to changes in atmospheric climate and nitrogen deposition. *Global Biogeochemical Cycles*, *27*(3), 650–663.